Late Drainage Along Portions of Samara Valles, West of Jones Crater, Margaritifer Terra, Mars

J. A. Grant[1], R. Manogaran[2], and S. A. Wilson[1]

[1]Smithsonian National Air and Space Museum, Center for Earth and Planetary Studies, 6th at Independence SW, Washington, DC, 20560
[2]Louisiana State University, Department of Geology and Geophysics, E235, Baton Rouge, LA 70803

Abstract

Relatively pristine valley segments along medial-to-distal Samara Valles in Margaritifer Terra likely originate within the continuous ejecta west of the Late-Hesperian Jones impact crater. Valley expression between a ~46 km^3 upper basin and a ~7 km^3 lower basin is typically well-incised with smooth walls and a relatively uniform width-to-depth, but elsewhere varies from well-incised to diffuse and some segments appear anastomosing or truncate one another. Many are more than a kilometer across and 100s of meters deep and display interior terraces and depositional forms. More pristine segments continue north and are associated with finely layered, alternating dark- and light-toned deposits well beyond Jones ejecta. Basins are approximately bound by the -1275 m MOLA contour and the upper basin displays benches and partially filled craters near and below that elevation. Lower interior surfaces of the upper basin are not incised, expose relatively light-toned discontinuous deposits, include polygonal fractures, and are locally Mg/Fe phyllosilicate-bearing. We interpret the formation of the relatively pristine segments as the result of water from impact-melted ice in and under the Jones ejecta draining westward, with some filling the upper basin. Water accumulated over a period of months to years before overtopping the divide and draining at rates perhaps on order of 10^4 m^3s^{-1} before filling and overwhelming the lower basin and breaching two additional local divides. Drainage persisted for a period of years at most and then

ceased. If correct, our model indicates a geologically brief interval of transient potentially habitable environments relatively late in Mars history that was likely unrelated to global climate.

Keywords: Mars, surface; Mars, climate; Geological processes, Mars

1. Introduction

The Margaritifer Terra region (**Fig. 1**) hosts a diversity of channels, valleys, and alluvial fans that record a long history of aqueous processes on Mars (e.g., Baker, 1982; Baker et al., 1992). The valley systems in Margaritifer Terra drain nearly 10% of the planet (Banerdt, 2000) and attest to the significance of this region in Martian geologic and fluvial history. The regional topography and structure are controlled by the axis of the Chryse trough that roughly divides the region and is part of a large circum-Tharsis depression (Phillips et al., 2001). In addition, there are several large, ancient, multi-ringed impact basins that include the Holden and Ladon basins (Schultz et al., 1982; Schultz and Glicken, 1979; Frey et al., 2008) (**Fig. 1**). Drainage features on the western flank of the Chryse trough are dominated by the Uzboi-Ladon-Morava (ULM) outflow system that incises between and fills ancient multi-ringed impact basins from its head in Argyre to its termination in Margaritifer basin (Salvatore et al., 2016; Wilson et al., 2022). Numerous valley systems are radial to the large basins on the western side of the Chryse trough (Saunders, 1979; Grant, 1987; 2000; Irwin et al., 2013; Weitz et al., 2023) and serve as minor tributaries to the ULM outflow system. By contrast, the eastern flank of the Chryse trough (**Fig. 1**) is incised by the Samara-Himera and Paraná-Loire valley networks that head in northern Argyre and western Noachis, respectively, and terminate in the Margaritifer basin to the northwest (Grant, 1987; 2000).

Geologic and geomorphic mapping defines a long history of fluvial incision and resurfacing by a variety of processes in Margaritifer Terra (Saunders, 1979; Grant, 1987; Rotto and Tanaka, 1995; Grant et al., 2009; Irwin et al., 2013; Tanaka et al., 2014; Wilson and Grant, 2018; Wilson et al., 2022; Weitz et al., 2023). Mapping provides a framework for evaluating the timing and relative importance of how major geologic events and processes shaped the landscape over time. In this region, the topography associated with the ancient Holden and Ladon impact basins, the Chryse trough, and relief created by subsequent impact craters defined the location and extent of basins and the evolution of their associated drainages, including the extensive Samara-Himera and Paraná-Loire valley networks (**Fig. 1**). The drainage basins encompassing these valley systems, which cover more than 540,000 km^2 (Grant, 1987; 2000; Grant and Parker, 2002), preserve the highest regional density of valleys on Mars (Grant, 2000; Hynek et al., 2010; Hynek, 2015; Alemanno et al., 2018) and have been the subject of morphometric (e.g., density) and hypsometric (basin area versus elevation characteristics) analyses (e.g., Grant, 2000; Grant and Fortezzo, 2003). Like most valley networks on Mars (e.g., Carr, 1995; 1996; 2006; Carr and Chuang, 1997; Fassett and Head, 2008; Alemanno et al., 2018) the Samara-Himera and Paraná-Loire systems largely formed in the late-Noachian into the Hesperian (Grant 1987; 2002; Grant et al., 2009; Irwin et al., 2013). Samara Valles heads in northern Argyre at a prominent ridge and the expression of the proximal-to-medial downstream trunk valley and major tributaries up to the vicinity of the southern edge of the continuous ejecta surrounding Jones crater is degraded (**Figs. 2 and 3**). Nevertheless, evidence of later fluvial activity in some valleys within Margaritifer Terra is preserved (Baker and Partridge, 1986), such as along the medial and lower reaches of Samara Valles beginning on or near the continuous ejecta southwest of Jones crater (Mangold et al., 2012) and extending well to the north of the crater and associated ejecta deposits.

Jones (19°S, 341°E) is a Late Hesperian (Parker, 1985; Mangold et al., 2012) ~90 km-diameter impact crater located between the medial sections of Samara and Loire Valles (**Fig. 1**). Jones crater, its interior alluvial fans largely on the northeast and east walls, and the few surrounding valleys have been the focus of prior studies related to crater degradation as a function of changing climate (e.g., Mangold et al., 2012). Jones formed on a northwest sloping surface along one of the Ladon impact basin rings immediately east of the Chryse trough axis (**Figs. 1-3**). As a result of this pre-existing topography, a pronounced N-S trending topographic low lies immediately west of the crater (**Fig. 3**). Although few valleys incise the exterior of the Jones crater rim and ejecta, topography on the western flank of Jones defines multiple small basins that may have filled and drained (**Fig. 4**). In addition, the section of Samara Valles immediately to the southwest, west, and downstream of Jones crater clearly incises Jones crater ejecta (Mangold et al., 2012) (**Fig. 3**) and appear more pristine than degraded valley segments further upstream (to the south) (**Fig. 5**) that are beyond the edge of the continuous ejecta (which extends approximately one crater diameter beyond the rim of Jones, see **Fig. 2** and Wilson and Grant (2023)). An additional tributary segment of the Loire valley system to the northeast of Jones crater was also proposed to be relatively pristine and incise Jones ejecta (Mangold et al., 2012; **Fig. 2**), but close examination of images covering the valley indicates it is buried by, and therefore predates, the Jones impact event. Because the relatively more pristine valley segments west of Jones crater originate near or within and incise into the Jones ejecta deposit, they can be no older than Late Hesperian and are likely younger than the more degraded portions of the system located further upstream to the south.

Deciphering the cause of late fluvial activity, and whether it relates to regional versus local geologic processes and (or) climate, is important for our broader understanding of the evolution of fluvial activity on Mars. Here, we focus on the morphologic evidence for late fluvial activity along Samara Valles southwest, west, and downstream of Jones crater, consider causal mechanisms and duration, and evaluate any constraints late aqueous activity may place on climate and habitability.

2. Data and Methods

Analysis of both the degraded and relatively pristine valleys relies mostly upon interpretation of Mars Reconnaissance Orbiter Context camera (CTX) (Malin et al., 2007; Dickson et al., 2018), High Resolution Imaging Science Experiment (HiRISE) image data (McEwen et al., 2007), and Mars Orbiter Laser Altimeter (MOLA) topographic data (Smith et al., 2001), supplemented by lesser Thermal Emission Imaging System (THEMIS) (Christensen et al., 2001; Edwards et al., 2011) and Compact Reconnaissance Imaging Spectrometer (CRISM) (Murchie et al., 2007) data for selected locales. We note that interpretations made from HiRISE images were completed using full image resolution, whereas the images presented in the figures herein are at lesser resolution to incorporate features of interest while providing broader coverage for context.

Volume estimates of impounded water in basins between some relatively pristine segments were derived using the Mars MGS MOLA – MEX HRSC Blended global DEM. A contour (e.g., -1275 m) was highlighted, and a shapefile was created in ArcGIS around it to create an enclosed basin evaluated using the Spatial Analyst Tools (Extraction, Extract by Mask) to extract the elevation data within the enclosed basin. The 3D analyst tool (functional surface, surface volume) was then used to calculate the volume of the raster with a reference plane of "below" and a plane height of selected elevation (e.g., -1275 m).

3. Observations and Interpretations

3.1 Character and Distribution of Pristine Samara Valles Segments

We observe relatively pristine morphology that can be traced continuously within valley segments on the west exterior of Jones crater as compared to most or all segments further south and beyond the Jones continuous ejecta (**Figs. 2 and 5**), The criteria we use to identify the relatively pristine valleys includes: (1) preservation of small scale (typically tens to hundreds of meters across, see **Fig. 4**) interior deposits and terraces, (2) valley floors that have relatively few impact craters, (3) valley floors that are typically incompletely buried by post-valley fill, and (4) bounding valley walls that are smooth, straight-to-curvilinear expressing limited spurs-and-chutes (in plan view). Relatively pristine valleys express a fairly uniform width ratio (with the exception of the most headward-most segments and where drainage crosses basins) By contrast, valley segments referred to as degraded (**Fig. 5**) possess valley floors that are typically covered by eolian fill, but in examples where the valley floor is exposed, they display relatively more impact craters. Further, degraded valleys reveal few or no obvious interior fluvial deposits and terraces, possess walls often marked by erosional spurs-and-chutes, display more irregular valley outlines (in plan view) and more variable width to depth ratios than the larger more pristine segments. There are examples of valleys that we identify as relatively pristine that do not display all of the morphologies noted above and there are also examples of segments identified as degraded where some degraded attributes are not present. There are also a few other valleys that we do not classify as either due to the absence of a clear fluvial signature. Our characterization as relatively pristine versus degraded relies on the presence or absence of most of the suite of identified characteristics and can be somewhat subjective. Nevertheless, we find that valley segments assigned as relatively pristine originate near the southern margin of the continuous ejecta surrounding Jones crater (**Fig. 2**) and extend northward for ~350 km to the west and north of the crater. Coupled with their incision of the ejecta around Jones crater, these attributes are indicative of late fluvial activity within Samara Valles along a ~350 km stretch west of Jones crater.

The downstream termination of the relatively pristine valley segments occurs where more substantial infilling and (or) mantling creates a transition to a more degraded and indistinct appearance to the north (**Fig. 4**), south of a younger volcanic construct that obscures the valley near its possible entry point into Margaritifer basin (Wilson et al., 2022). The upstream origination of the relatively more pristine valley segments is also uncertain. A southernmost incised segment and associated downstream lobate deposits is closest to the margin of the continuous ejecta (**Fig. 6**). Some areally small, smooth surfaces on the distal ejecta that lack evidence of clear incision may be graded alluvial surfaces. The lack of evidence for numerous smaller-sized contributing valleys may be related to post incision degradation that obscures their identification and (or) limited incision due to dominantly groundwater versus runoff versus groundwater sourcing, and (or) discontinuous HiRISE image coverage. One example of a valley segment just over ~150 km south of Jones, beyond the continuous ejecta, expresses attributes of both relatively pristine and degraded valley segments (**Fig. 7**). Here, a fairly straight and more deeply incised central reach heads near multiple flat-topped features, but is bounded within by a wide and irregular outline (in plan view). Unlike relatively pristine segments further north, however, it is unclear whether the flat-topped features are eroded remnants of material once filling the valley (Wilson et al., 2023) or associated with late discharge, as they are relatively high standing and bounded by steeper edges on the downstream, valley interior as well as the valley wall facing sides. Although this valley segment (**Fig. 7**) is likely within the range impacted by discontinuous ejecta from Jones (e.g., Melsoh, 1989), the downstream extension of the valley expresses a more degraded expression that continues north to near the southern margin of the continuous ejecta deposit and is more typical of what is observed further south. Hence, while the origination of the relatively pristine segments remains uncertain, it is unlikely to extend more than about two crater diameters south of Jones and is more likely confined to within the distal edge of the Jones crater continuous ejecta deposit.

The furthest upstream recognizable relatively pristine valley segments (**Fig. 6**) are typically <600 m across and express limited incision (<15 m), but clearly cut into the Jones ejecta deposit (**Fig. 6**). These upstream segments are smaller than those further downstream and transition into a series of coalesced lobes (**Fig. 6**) before becoming less distinct at the margin of a topographic basin southwest of Jones (termed "upper basin," see **Figs. 2-4**). Where the valley crosses the upper basin divide near the northeast corner it reemerges at a much larger scale that is over 1 km wide, hundreds of meters deep (**Fig. 8**) and displays multiple examples of interior terraces and apparent depositional forms (**Fig. 9**). Further downstream, the valley expression varies from distinct and well-incised to locally diffuse, indistinct, or braided (**Fig. 10**). The relatively pristine valley then traverses a second, smaller, topographic basin (termed "lower basin," see **Figs. 2-4**) west-northwest of Jones where reaches appear anastomosing (**Fig. 11**) before becoming deeply incised and sometimes truncating one another immediately downstream (**Fig. 12**). Although enclosed basins downstream of the lower basin are not present, two east-west ridges create local divides that are breached and may have influenced the form and location of the downstream valley segments. Sections of the relatively more pristine segments probably follow the older, original Samara Valles system given the large scale of the system that would have followed the pre-Jones impact topographic low along the axis of the Chryse trough (for example, where it emerges through the divide on the northeast side of the upper basin and southwest of Jones, **Fig. 8**). Some valley reaches are more than a kilometer across and 100s of meters deep in their entirety (**Figs. 9-11**). Further north beyond the Jones ejecta, the valley segments are less confined, less-well incised, and sometimes appear disrupted (**Fig. 13**), but sediment transported by the discharge apparently contributed to finely layered, alternating dark- and light-toned deposits partially filling the trough axis and a crater breached by the system even further downstream (**Fig. 14**). There are few tributaries to the relatively pristine segments, with the possible exception of poorly incised and integrated drainages entering from basins on the western flank of Jones (e.g., at a bench where the trunk valley turns from north to west, see **Figs. 2 and 10**).

Many sections of the relatively pristine valley system are flanked by apparent depositional forms and (or) erosional terraces/benches and there are multiple abandoned segments downstream of the lower basin that suggest periods of laterally shifting flow within the valley as it down cut. For example, erosional terraces occur along the northwest side of the trunk valley after it emerges from the upper basin, near the turn back to the west at the toe of the Jones crater flank, in an alternating pattern further downstream and above lower basin, and then as series of elongate features within the main valley below the lower basin **(Figs. 4, 9-11**). Immediately downstream of the lower basin, a series of valley segments occur at differing elevations where they cross the local east-west divides, with lower elevation valleys consistently truncating those at higher elevations (**Figs. 4, 12**). Additional deposits and terraces occur within and between the valleys at varying elevations and likely record changing direction and (or) levels of discharge as basins and divides were breached (**Figs. 4, 12**). While the relatively pristine segments are valleys, associated drainage along the interior channel reached maximum depths recorded by lowermost terraces and possible depositional forms bounding the valley walls. Further, the preservation of subtle erosional and probable depositional features implies that downcutting dominated formation that was accompanied by limited lateral retreat of valley walls. Hence, significant parts of the floors of the relatively pristine valley segments were occupied by active channels.

3.2 Local Basins and Associated Deposits

The larger, upper basin southwest of Jones (**Figs. 2 and 15**) is generally defined by the -1275 m MOLA contour, has long dimensions of approximately 50 x 60 km though is quite irregular in shape, encloses a volume of ~46 km^3 (**Fig. 15**), and expresses multiple isolated local lows below the level of the outlet. The smaller, lower basin west-northwest of Jones is similarly defined by the

-1275 m MOLA contour, has long dimensions of approximately 20 x 25 km, is irregular in shape, and encloses a volume of ~7 km^3 (**Figs. 2 and 16**).

The upstream entry into the upper basin is marked by the coalesced lobes of material associated with the initial expression of the relatively pristine valley segments that terminate at or close to the -1275 m elevation (**Fig. 6**). The floor of the upper basin is otherwise not incised except for a deep and wide outlet valley heading immediately upstream of the ridge forming the enclosing divide on the northeast corner (**Fig. 8**). A bench occurs just below the basin-side crest of the divide northwest of the origination of the wide, exit valley (**Fig. 8**). The intervening floor of the basin displays a variety of features, sometimes covered by a relatively thin sequence of relatively light-toned layered deposits, and local sets of polygonal fractures that resemble desiccation cracks (**Fig. 18**). Some locations on the floor and near the divide are marked by partially filled craters (**Fig. 17**) whose higher rims in the latter case display benches close to the -1275 m divide (**Fig. 18**). The elevation of some benches (**Fig. 18**) is near, but below -1275 m, indicating they may have been modified due to tectonic or other process or been cut during the filling or draining of the basin. Collectively, however, we interpret the occurrence of these features as consistent with flooding of the upper basin to an elevation near -1275 m.

Putative chloride-bearing materials have been detected in Margaritifer Terra using THEMIS data and are often associated with polygonally fractured surfaces but are not identified in the ejecta blanket of Jones crater (Osterloo et al., 2008; 2010; Glotch et al., 2010; Leask and Ehlmann, 2022). There is limited CRISM coverage within the upper basin and even less that include longer wavelength reflectance data (Murchie et al., 2007), but a single CRISM image covering the deepest portion of the upper basin suggests Fe/Mg phyllosilicates are present in the relatively light-toned layered deposits there (**Fig. 17**). Interestingly, a CRISM image inside the west rim of Jones crater

(FRT0000B771_07_IF164L_TRR3) and on an alluvial fan in the northern interior of the crater (FRT000168B6_07_IF164L_TRR3) show limited or no evidence of widespread Fe/Mg phyllosilicates. Therefore, it remains uncertain whether the phyllosilicates in the upper basin are part of a regional deposit on the flank and exterior of Jones or appear as a more isolated occurrence perhaps formed autochthonously within the basin.

In contrast to the upper basin, the relatively pristine valley entering the smaller, lower basin is more than a kilometer wide and 100s of meters deep (**Fig. 4**). That main valley continues to the northwest before broadening into a series of fan-shaped deposits separated by anastomosing incised sections of the valley (**Figs. 4, 11, 12**). A smaller distributary valley whose floor is above the main valley floor splits off the main valley just after entry into the basin and is oriented first northeast and the turns to the northwest before terminating in subtle lobes of deposits (**Fig. 4**). The widest and deepest valley splits and exits the lower basin in three locations along the north and northwest divide. The largest of these is at the lowest elevation and is associated with the anastomosing valleys that separate the fan-shaped deposits (**Figs. 4 and 11**). The other two valleys exiting the lower basin are at the northwestern corner and are smaller in cross section and at higher elevation. The lower, larger valley truncates both where it traverses west before turning back to the east and eventually to the north after crossing the two local east-west divides (**Fig. 12**). Unfortunately, there are no CRISM images covering the lower basin or any other section of the more pristine drainage segments.

3.3 Late Discharge Through Relatively Pristine Valley Segments

The form and distribution of the relatively pristine valley segments and the expression of the floors and divides of the upper and lower basins provide clues regarding the nature of late discharge through the system. The smaller scale and length of the pristine valley segments upstream of the upper basin implies comparatively less discharge was sourced from further south as compared to that shaping the larger valley segments further downstream. Moreover, the occurrence of coalesced lobes of material near the -1275 m MOLA contour and the paucity of additional tributaries or incision below that elevation within the upper basin indicates that the upstream valley dominantly sourced the runoff that ponded near that elevation before overtopping and exiting through a breach in the northeast basin divide. The presence of relatively lighter-toned layered and at least locally Mg/Fe phyllosilicate-bearing deposits (**Fig. 17a**), partially buried craters, polygonal fractures in the basin (**Fig. 17b**), and benches around higher topography elsewhere around the basin divide (**Fig. 18**), support the interpretation that the basin was flooded to an elevation of around -1275 m.

The valley draining through the northeast upper basin divide is much larger than the smaller, upstream valley sourcing basin filling. This implies that peak discharge out of the basin exceeded that flowing into the basin and was likely associated with overtopping and downcutting the divide, thereby allowing downstream drainage of impounded water. Discharge out of the upper basin may have been incomplete due to water remaining in local lows within the basin, but water that did drain continued northeast towards the base of the west flank of Jones crater before turning north, then west, then northwest and entering the lower basin (**Fig. 4**). A series of depositional forms and (or) terraces within the valley represent surfaces that were abandoned as downcutting continued. At least one of these features, immediately downstream of the outlet from the upper basin, abuts the northern valley wall and displays a steep channel-ward side that tapers to a steep front on the downstream end. We interpret this and other broadly comparable features to be large bar-forms within the valley (**Figs. 8b, 9, 10**) and, if correct, points to the record of sediment being fluvially transported within the valley.

Flow entered the smaller, lower basin through a set of branching distributaries to the northeast and predominantly to the northwest. As the flow decelerated, the transported sediment load was deposited as a series of fans and as a smaller, steep fronted deposit near the downstream divide, likely as a fan-delta within the rapidly filling basin. As discharge continued, it overwhelmed and overtopped the confining northern divide of the lower basin, first at two locations near the northwest corner and then further to the east. Downcutting of the divide led to dominance of the eastern outlet, abandonment of the northwest outlets that created a series of up to four terraces (**Fig. 4**) and led to incision and downstream redistribution of lower basin fan sediments as water drained northward. A few large blocks that are barely resolvable at HiRISE scale near the downstream end of the lower basin fan point to high rates of discharge during drainage of the basin (**Fig. 11**).

As the lower basin continued to drain, water crossed the lower basin divide further downstream and well to the west before turning eastward and then northeast and crossing a local divide (**Fig. 4**). There appears to have also been an incipient breach of the second local downstream divide further to the east that was abandoned as more significant discharge through the main valley resulted in more rapid downcutting and further consolidation of drainage into a single valley. As flow out of the lower basin consolidated, however, increased incision carved a new valley more to the east that took advantage of the newly formed divide breaches and caused abandonment of adjacent segments (**Figs. 11, 12**).

Further downstream/to the north, there is less confining topography along the sides of the trough axis, thereby allowing flow to have expanded laterally (**Fig. 3**). The valley form responded by becoming less incised, more diffuse, and marked by multiple degraded, possible bar-forms and marginal relatively lighter and darker toned deposits (**Figs. 4, 13, 14**). Close examination of the central valley along the northern segments reveals a surprisingly etched appearance and suggests more degradation of the valley, perhaps related to the presence of finer-grained and (or) more erodible materials. As noted, the valley begins to display an even more degraded expression well to the north that rivals that upstream of the relatively pristine valley segments (**Fig. 14**) and may be due to degradation associated with nearby younger volcanic activity and emplacement and (or) redistribution of associated materials (**Fig. 19**).

3.4 Magnitude and Duration of Discharge Along the Relatively Pristine Valley Segments

Several aspects of the relatively more pristine valley segments suggest that their formation was the result of geologically short-lived discharge of water sourced primarily in and just upstream and downstream of the upper basin within the Jones crater ejecta deposit. First, the relatively pristine valley segments originating upstream of the upper basin and within the Jones ejecta are smaller and poorly incised relative to valleys segments downstream of the upper basin. And associated coalesced, lobate deposits occurring around the -1275 m MOLA contour are relatively small (**Figs. 4, 6**) compared to intra-valley depositional forms further downstream and in the lower basin (**Figs. 4, 8b, 9, 10**). By contrast, a much larger valley emerges through the divide on the downstream side of the upper basin that maintains a roughly similar appearance in cross-section beyond the lower basin. The floor of the valley in the vicinity of the sharp turn to the west near the base of the Jones crater flank (**Figs. 9, 10**) appears somewhat braided consistent with increasing sediment load during decreasing discharge. Finally, the floors of the upper and lower basin show no evidence of incision following initial drainage that would be expected if there were multiple and (or) persistent through flow. Collectively, and coupled with the paucity of obvious tributaries (with the possible exception of a tributary entering from the west flank of Jones, see **Figs. 2, 9, 10**), we interpret these attributes to indicate valley incision below the upper basin to be the result of water in the upper basin breaching the downstream divide and rapidly draining (i.e., hydrograph likely narrow and high peaked) to create the morphology observed today. The lack of evidence of incision across the floor of both the upper and lower basins associated with post-drainage flow or recharge, such as the presence of an interior channel across the floor or within valley segments downstream of the basins, indicates flow ceased following drainage of the basins (which may have been incomplete from the upper basin due to internal lows).

Estimates of discharge along the relatively pristine valleys can give additional insight into the duration of drainage that has implications for the cause. For example, discharge estimates that point to a geologically brief (weeks, months, years) period of drainage are consistent with sourcing related to local impact, volcanic, or even tectonic events. Discharge estimates more consistent with geologically longer term (hundreds to thousands of years) drainage would be more consistent with climate driven sourcing of activity. With that in mind, and assuming much of the valley bottom was occupied by an active channel, we estimate associated channel dimensions and gradients using images and topography from MOLA shot points to derive order of magnitude estimates of the discharge from the upper basin and provide additional insight into the probable duration of associated aqueous activity. We appreciate that there are large potential errors associated with such calculations (e.g., Burr et al., 2010; Jacobsen and Burr, 2018) that include uncertainties in the amount of fill in the valley, the assumed wetted cross-section of the channel within the valley, the coarse spacing and limited number of MOLA shot points that are available to constrain local channel depths and gradients, and how much erosional back wasting of valley walls has occurred, among others. Nevertheless, we suggest that the occurrence of likely depositional forms and terraces give sufficient clues regarding past channel dimensions for use as a guide in exploring paleodischarge using these data over a range of values in order to place crude limits on how long it may have taken the upper and lower basins to initially fill and subsequently drain. In appreciation of these large uncertainties, we also consider the implications of our discharge estimates on the duration of activity if they are either one or even two orders of magnitude higher or lower than what we estimate.

We considered multiple methods for estimating discharge that included models for post-impact hydrothermal systems (e.g., as described in Barnhart et al., 2010) and methods for estimating discharge as described in Konsoer et al. (2018), Wilson et al. (2004), Burr et al. (2010), and Mangold et al. (2012). We excluded models for post-hydrothermal systems (Barnhart et al., 2010) because they are relevant for understanding persistent discharge within rather than outside newly formed craters. We also excluded methods applied to equilibrium bank full drainage flow (e.g., Konsoer et al. (2018) and Burr et al. (2010)) because the relatively pristine valley segments were likely experiencing active incision based on occurrence of abandoned segments, the widespread occurrence of interior terraces and putative depositional forms, and channels that covered much, but not the entirety of valley floor. Here, we estimate discharge using the Darcy-Weisbach equation (Wilson et al., 2004) as modified by Mangold et al. (2021) to yield,

$$Q = HWV = A\left({}^{8RgS}/_{f_c}\right)^{0.5} \quad (1)$$

where Q is the discharge ($m^3 s^{-1}$), A is the flow depth (H, in m) times the flow width (W, in m), V is the flow velocity ($m s^{-1}$), g is the gravitational acceleration ($m s^{-2}$), S is the slope (dimensionless), f_c is the Darcy-Weisbach friction factor (dimensionless), and R is the hydraulic radius (the ratio of the cross-sectional area A to the wetted perimeter P for either a rectangular or triangular cross section, respectively). For the channels studied here, R is assumed to equal H because W is much greater than H after Wilson et al. (2004).

For the Friction factor (f_c), we used predictors for a sand bed, gravel bed, boulder bed, and upper regime sand bed (equations 13-15 and 7b in Wilson et al., (2004), respectively). After Mangold et al. (2021) we also calculated the f_c for a gravel bed using equation 13 in Kleinhans (2005) that incorporates channel gradient. We derived estimates using these equations based on grain sizes observed at the Viking and Pathfinder landing sites after Wilson et al. (2004) that we believe may be good analogs: the relatively pristine valleys incised into and transported fragments of the Jones crater ejecta (and perhaps underlying megaregolith) whose average properties are predictable based on fragmentation laws (e. g., Brown, 1989; Melosh, 1989), will include a coarse fraction, and therefore approximate the poorly sorted range of fragment sizes observed at those landing sites. We also made estimates using the grain sizes observed at Jezero crater after Mangold et al. (2021) for completeness, though it is uncertain whether drainage in the depositional setting at Jezero is analogous to that occurring along the relatively pristine valleys. After Wilson et al. (2004) for the Pathfinder and Viking landing sites and D_{50} (median gran size) and D_{84} (84^{th} percentile used to represent the coarse fraction) values,

Sand Bed $$(8/f_c)^{1/2} = 8.46(R/D_{50})^{0.1005} \quad (2)$$

Gravel Bed $$(8/f_c)^{1/2} = 5.75\log_{10}(R/D_{84}) + 3.514 \quad (3)$$

Boulder Bed $$(8/f_c)^{1/2} = 5.\ 62\log_{10}(R/D_{84}) + 4.0 \quad (4)$$

Upper regime $$(8/f_c)^{1/2} = 7.515(R/D_{50})^{0.1005}\ S^{-0.03953}\sigma_g^{-0.1283} \quad (5)$$

In (5), upper flow regime corresponds to a plane bed with transport and having antidunes and chutes and pools, whereas σ_g is the geometric standard deviation of the bed clast size distribution, dimensionless (the dimensionless number equal to the ratio of the mean size to the size one standard deviation away from the mean).

After Kleinhans (2005) as evaluated in Mangold et al. (2021) for Jezero crater and D_{50} (median gran size) value,

$$\text{Gravel Bed} \quad (8/f_c)^{1/2} = 2.2(R/D_{50})^{-0.055}s^{-0.275} \quad (6)$$

For reference, sand grains are 0.0625-2.0 mm, gravel is 2.0 to 80 mm, and boulders are coarser than 256 mm across (Folk, 1980).

Channel width was estimated along eight profiles (**Fig. 4**) approximately perpendicular to margins identified by locations where morphology (e.g., lowermost occurring putative depositional forms or terraces, (e.g., **Fig. 9**)) and MOLA shot points indicate a transition to lower, intervening elevations (Supplemental Data File, see Grant et al., 2023). The elevation of the channel margins and floors were estimated using an average of MOLA shot points on the channel margins and floors that are located as close as possible to the selected profiles (Supplemental Data File, see Grant et al., 2023). Finally, channel depth was estimated using the difference in elevation between the channel margin and channel floor. Using these estimated channel widths and depths, we then assumed both rectangular and triangular channel cross sections along the profiles. Although the spacing of MOLA data is coarse relative to the scale of the relatively pristine valleys, we find that using the average of multiple shot points in close proximity to and along our profiles is sufficient for supporting order of magnitude estimates of discharge. Given additional uncertainties in channel dimensions (e.g., the amount of fill) we do not rely on more detailed cross sections for our estimates (e.g., CTX Digital Elevation Models). Nevertheless, discharge estimates based on assumed rectangular sections are likely too high because they do not incorporate shallowing from the channel thalweg to the margin. As a result, we emphasize the lower discharge estimates based on assumed triangular cross sections in our consideration of the possible duration of drainage. Finally, we ignore potential contributions to discharge from groundwater which may be very significant (given the paucity of tributaries associated with surface runoff). Study of ejecta deposits around Meteor Crater on Earth, which may provide an analog for the properties of ejecta around Jones, reveal that it has a high infiltration capacity and is highly permeable (Grant and Schultz, 1993) and could enable efficient subsurface drainage of water in the Jones ejecta that may also contribute to basin infilling and runoff.

Resultant channel width and depth estimates for our eight selected profiles across the channel are between 201-586 m and 10-11 m, respectively, upstream of the upper basin (**Table 1**, **Fig. 4**, profiles 1, 2 that are shown by single line due to their close proximity). Estimated channel dimensions downstream of the upper basin are larger. As summarized here and in **Table 1** (additional details are in the Supplemental Data File, see Grant et al., 2023), immediately downstream of the upper basin outlet breach the channel is estimated to be 840 m wide and 73 m deep (**Fig. 4**, profile 3), though the steep walls and fill on the valley floor make the channel dimensions and this estimate the most uncertain. Slightly further downstream (**Fig. 4**, profiles 4-6) the widths and depths are estimated at 750-909 m and 19-32 m, respectively. Occurrence of the relatively flat-topped depositional form or terrace on the channel margin coupled with the relative uniformity of the elevation along this section of the channel floor suggest these profiles may be most realistic. Further upstream of the lower basin estimated widths are 620 m and depths are 11-15 m (**Fig. 4**, profiles 7-8).

For channel gradients (**Table 1**), we selected individual MOLA shot points located along the central valley floor and measured the intervening distance along the channel (Supplemental Data File, see Grant et al., 2023). The estimate for the gradient upstream of the upper basin is 5.0 x 10^{-4} (**Fig. 4**, profiles 1, 2). Downstream of the upper basin the estimated gradient is 4.2 x 10^{-3} just below the upper basin outlet breach (**Fig. 4**, profile 3). Further downstream (**Fig. 4**, profiles 4-6) the gradient measured along the channel averages 3.2 x 10^{-3} (depending on the choice of MOLA shot points along the floor). Still further downstream (**Fig. 4**, profiles 7-8) the measured gradient was measured along the channel floor passing through both profiles and is 4.0 x 10^{-3}.

We derived discharge estimates (**Table 1**) using these values and assumed rectangular and triangular cross-sections, along-channel gradients, and the friction factor for various bed types (equations 5-9) in (equation 4). In general, discharge estimates for a given cross-section and gradient only vary by 15% or less in response to the use of differing friction factors and by 10% or less in response to use of grain sizes from the Pathfinder/Viking landing sites (after Wilson et al., 2004) versus Jezero crater (after Mangold et al., 2021, see **Table 1**, Supplemental Data File, Grant et al., 2023). Because of this, our results are averaged for the Pathfinder/Viking landing sites and for Jezero crater as they have less influence on the magnitude of the discharge than variations and likely associated uncertainties in the channel dimensions (see **Table 1**, Supplemental Data File, Grant et al., 2023). For assumed rectangular cross sections along the profiles (**Table 1**), the short segment upstream of the upper basin (**Fig. 4**, profiles 1-2, **Table 1**), the average discharge estimates range between 0.4 x 10^4 m^3s^{-1} and 1.1 x 10^4 m^3s^{-1} using the Pathfinder/Viking grain sizes and 0.4 x 10^4 m^3s^{-1} and 1.0 x 10^4 m^3s^{-1} for the Jezero crater grain sizes. By contrast, the average discharge estimates downstream of the upper basin are greater (**Fig 4, Table 1**). For the Pathfinder/Viking and Jezero grain sizes, respectively, the estimates are (a) 91 x 10^4 m^3s^{-1} and 85 x 10^4 m^3s^{-1} near the outlet breach (profile 3), (b) 11-20 x 10^4 m^3s^{-1} and 9.4 x 10^4 m^3s^{-1} to 19 x 10^4 m^3s^{-1} profiles 4-6), and (c) 3.4-5.6 x 10^4 m^3s^{-1} and 3.2-5.2 x 10^4 m^3s^{-1} (profiles 7-8) just above the lower basin.

For assumed triangular cross sections (**Table 1**), along the short segment upstream of the upper basin (**Fig. 4**, profiles 1-2, **Table 1**) the average discharge estimates range between 0.1-0.4 x 10^4

m^3s^{-1} and 0.1-0.3 x 10^4 m^3s^{-1} for Pathfinder/Viking and Jezero grain sizes, respectively. Average discharge estimates downstream of the upper basin are 30 x 10^4 m^3s^{-1} and 28 x 10^4 m^3s^{-1} near the outlet breach for Pathfinder/Viking and Jezero grain sizes, respectively (**Fig. 4**, profile 3, **Table 1**), 3.3-6.7 x 10^4 m^3s^{-1} and 3.1-6.3 x 10^4 m^3s^{-1} just downstream adjacent to the large depositional form for Pathfinder/Viking and Jezero grain sizes, respectively (**Fig. 4**, locations 4-6, **Table 1**), and 1.1-1.8 x 10^4 m^3s^{-1} and 1.0-1.7 x 10^4 m^3s^{-1} just above the lower basin for Pathfinder/Viking and Jezero grain sizes, respectively (**Fig. 4**, profiles 7-8, **Table 1**).

As noted, the sizeable range in estimates for both the assumed rectangular and triangular channel cross sections undoubtably reflects the considerable uncertainties in the various parameters measured and employed in these calculations; they are not necessarily precise predictions of discharge and should not be regarded as such. Instead, we use the general magnitude of the estimates that are considered to one and two orders of magnitude higher and lower to get a sense of the impact on, and reasonable duration of, the discharge along the relatively pristine valleys. We emphasize the average discharge values for the Pathfinder/Viking landing sites and Jezero crater (which are broadly similar, **Table 1**) based on assumed triangular channel cross sections for exploring the duration of discharge as they may best capture the relatively small effects of the range of possible grain sizes and likely shallowing towards the channel margins. We also exclude the discharge estimates for profile 3 due to our lower confidence in estimated channel dimensions at that location. With that in mind, and knowing that the various friction factors do not significantly change the discharge estimates, we consider possible constraints on the duration of discharge using an average discharge upstream of and into the upper basin of ~0.2 x 10^4 m^3s^{-1} and an average discharge below the upper basin (based on profiles 4-8) of ~3 x 10^4 m^3s^{-1}.

Taken by itself, the potentially lower average discharge of 0.2 x 10^4 m^3s^{-1} upstream of, and into, the upper basin could fill the 46 km^3 volume with water in about 9 Earth months. If our estimate is one or two orders of magnitude too low or too high, then the upper basin would have filled in mere days to as long as around 5 to around 60 Earth years, respectively. Significant groundwater contributions to infilling, as seems possible given the paucity of incised surface tributaries, would shorten the time needed to fill the basin. By contrast, the 3 x 10^4 m^3s^{-1} average discharge estimated downstream of the upper basin implies the entire 46 km^3 of water within could have drained in ~17 Earth days or over a period of ~6 months to close to 5 Earth years if discharge was one or two orders or magnitude lower than we estimate, respectively. Actual discharge from the upper basin may have been lower and (or) of shorter duration because the elevation of the outlet remains above the lowest points in the basin, thereby suggesting some water remained ponded in interior local topographic lows/depressions within the broader basin. The occurrence of some polygonal fracturing associated with relatively lighter-toned deposits on the basin floor is consistent with incomplete drainage of these lows followed by longer term evaporation of water remaining. By contrast, significant groundwater contributions to the active channels could have increased discharge into and out of the basin. Regardless, we believe that our consideration of discharge estimates over such a broad range that all yield geologically short durations for discharge almost certainly capture the potential effects of these possibilities.

Although the shape of the actual hydrograph during discharge is not known, even if peak flow was realized during as little as 1% of the upper basin drainage event, the overall duration would have been measured in years to decades at most. Therefore, despite large uncertainties in parameters related to the discharge estimates, we conclude that even the most extreme upper estimates of the duration of flow necessary to fill and drain the upper basin are on the order of years to decades and months to years, respectively, suggesting the valleys were active over a geologically brief period of time. Moreover, the juxtaposition of geomorphic features (i.e., because the floors of both the upper and lower basin and the entry fan into the upper basin are not incised) reveals no evidence of later discharge following initial basin drainage. Hence, we conclude that the flow responsible for the relatively pristine valleys occurred during a single, geologically brief event.

The small number and scale of possible tributaries to either the upper or lower basin, as exemplified by the possible tributary drainage entering from the western flank of Jones (**Figs. 3, 4, 10**), implies the smaller valley segment upstream of the upper basin dominated surface runoff contributions to filling. Moreover, the lobes of material at the downstream end of the smaller valleys suggests discharge was characterized by a fairly low sediment-to-water ratio. As noted, the filling of the upper basin may have varied, been filled via lesser discharge from upstream sources than we estimate here, and (or) been accompanied by significant groundwater contributions that could have greatly shortened the time needed for flooding. Nevertheless, the absence of intrabasin incision, no other putative deposits associated with any lower stands of water within the basins, and the small size of the coalesced lobate deposits fringing valley entry implies continuous infilling of the upper basin until overtopping of the downstream basin divide occurred.

The coalesced lobate deposits at the entry point into the basin and multiple benches at several locations around the upper basin are close to the -1275 m MOLA elevation of the basin divide. That may be consistent with a stable outlet where initial outflow was matching inflow for a time, but the small-scale of the coalesced lobated deposits at the entrance to the basin suggests such a scenario was not geologically long-lived if it occurred. The absence of recognizable benches or possible deposits at significantly lower elevation(s) within the basin further indicates that the water levels did not stabilize for any length of time during draw-down of the water in the basin. Finally, light-toned layered deposits within the basin are not extensively distributed and are relatively thin, only partially burying some craters. And while it is unclear how extensive Mg/Fe phyllosilicate-bearing sedimentation was, the inferred thin nature of basin deposits implies basin flooding did not likely persist for very long. These observations are all consistent with the lack of incision across the floor of the upper basin, including where the layered deposits occur (**Fig. 17**), and the cessation of flow following initial draining of the basin.

Collectively, we believe that these observations indicate that once the basin was filled and overtopped the downstream divide, outflow to the north and draw down of the water in the upper basin was continuous, but perhaps of variable discharge, and then ceased. By contrast, initial discharge into the upper basin may have been relatively smaller. Regardless, based on the scale of the lobate putative deposits associated with source channels and expansion of our discharge estimates to two additional orders of magnitude above and below our estimates indicates the basin could be filled in months to years at most, after which recharge effectively ceased. Similarly, initial and late flow out of the upper basin were probably less than during the peak discharges estimated from the channel dimensions herein. If such high peak discharges were achieved, they were not long-lived, as drainage of the upper basin and limited evidence for long-lived or stable water levels therein suggest it was drained over no longer than months to perhaps years before becoming inactive.

4 Discussion

4.1 A Model for Formation of the Relatively Pristine Valley Segments

Relatively pristine valley segments and incorporated channels along medial Samara Valles arise on the southwest and west side of Jones within the continuous ejecta deposit surrounding the crater and therefore post-date crater formation in the Late Hesperian. Comparably pristine valleys are not observed elsewhere around the crater or in the region (**Figs. 2 and 3**). The scale of the drainages upstream and below two basins on the ejecta suggest that the valleys were carved by high discharges of water over periods of no more than years and then ceased. Water associated with the formation of the relatively pristine segments continued northward and may have eventually reached Margaritifer basin (**Fig. 1**), though the ultimate fate of the water is uncertain.

High volume, short duration discharge coupled with the isolated occurrence of the relatively pristine valleys points to a local source of water rather than a regional or global climate-driven water source driven by synoptic precipitation. Volcanic activity is one possible source of water and heat that may have sourced the valleys, but the nearest structure is at the downstream end of the pristine segments and appears to have degraded rather than sourced the valleys (**Fig. 19**). Another possibility is that tectonic activity triggered release of subsurface water, but there is no evidence that the upstream sections of the relatively pristine valleys originate at a linear feature such as a fault or graben and there is no sign of surface collapse such as might be expected if there was significant discharge of water.

Another model, that may be consistent with the attributes of the relatively pristine Samara Valles segments, relates to late discharge sourced by melting ice and (or) water in and below the Jones crater ejecta after formation of the crater. This scenario has been proposed for formation of valleys with interior channels and a range of landforms around the more pristine and Amazonian ~140 km-diameter Hale crater (35.7°S 323.4°E) north of Argyre (Jones et al., 2011; El-Maarry et al., 2013; Grant and Wilson, 2017) and the ~235 km-diameter Lyot crater in Ismenius Lacus (Dickson et al., 2009; Weiss et al., 2017). An impact-melting induced drainage formation mechanism was previously suggested as a possibility for forming the pristine valley segments west of Jones crater (Mangold et al., 2012), but was not explored in detail. Around craters Hale and Lyot, water draining from and beneath the fresh, warm ejecta created a series of valleys and deposits and reactivated downstream valleys reaching well beyond the associated ejecta deposits (Dickson et al., 2009; Jones et al., 2011; El-Maarry et al., 2013; Grant and Wilson, 2017; Weiss et al., 2017).

For example, the suite of landforms surrounding Hale crater can be associated with water draining from the ejecta around the crater (Jones et al., 2011). Landforms include valleys with interior channels, lobate deposits and subtle distal ejecta deposits that are interpreted to be water-fluidized debris flows of ejecta mixed with water–ice-rich basin materials (El-Maarry, et al., 2013; Grant and Wilson, 2017). The fluidized flows around Hale typically originate within but extend well beyond the continuous ejecta (Jones et al., 2011) where they generally follow pre-existing topography and are observed around the crater. While the fluidized flows sometimes occur as leveed deposits on low relief surfaces, many occur as channels within valleys created by topography existing on the ejecta draped surface and (or) within pre-existing valleys beyond the continuous ejecta. One pristine channel within a preexisting valley north of the crater reaches all the way to Uzboi Vallis ~200 km to the north (Grant and Wilson, 2017). Although some valleys and incorporated channels at Hale are small when compared to the relatively pristine segments west of Jones, others are of comparable size and even larger. In one instance north-northwest of Hale, the peak discharge in a channel through a topographic constriction was estimated at over 10^5 $m^3 sec^{-1}$ (Grant and Wilson, 2017), exceeding most estimates for the relatively pristine segments west of Jones crater. Emplacement of the array of features surrounding Hale crater were hypothesized to have occurred within days of impact (Grant and Wilson, 2017), though it seems likely that drainage away from the crater continued along at least some channels for a longer time.

The lobate deposits at Hale are tens of meters thick, often express transverse rides on top, are fronted by digitate features, and typically occur at the end of channels, thereby inferring they are deposits associated with drainage through the channels. An array of more subtle features associated with the distal ejecta are typically less than 10 m thick and have volumes less than 0.5 km^3, suggesting they were fluidized and flowed when impacting the surface beyond the continuous ejecta (Grant and Wilson, 2017). Features directly comparable to the lobate deposits and subtle distal ejecta features may not be observed outside of Jones crater.

4.2 Are the Relatively Pristine Segments Along Samara Valles Related to the Jones Impact?

There are common attributes associated with the relatively pristine valleys and incorporated channel segments west of Jones crater and those occurring around the younger Hale and Lyot craters. For example, valleys around Jones appear to originate on the ejecta deposit but extend downstream well beyond its limit, have few associated tributaries, apparently formed during a brief period of high discharge following the Jones impact event, and then became inactive. In addition, models suggest (Squyres et al., 1992; Jones et al., 2011) it is possible that sufficient water ice may have been accommodated in the pre-impact and surrounding surface to source incision of the valleys west of Jones.

Although the amount of ice available for melting via the impact and by melting beneath the ejecta is poorly known, reasonable models for pore ice (e.g., Squyres et al., 1992) suggest it may have been sufficient to fill the upper and lower basins and source the relatively pristine valleys. For example, if there was 20% pore ice to a depth of 1 km in the pre-impact region where 90-km-diameter Jones crater formed, it would represent more than 1200 km^3 of ice that would have been excavated and melted during the impact. Even if 75% of the ice filling pores was vaporized during impact and only the ejecta in the quadrant southwest of Jones is considered, more than 75 km^3 of ice would have been emplaced with the ejecta. If emplacement of the warm ejecta caused melting in the uppermost 2 m beneath the ejecta to one crater diameter beyond the Jones crater rim, that would increase the inventory of water from melted ice by an additional 5 km^3 to more than 80 km^3 in the quadrant southwest of Jones. Vaporization of more ice during impact or very rapid refreezing after impact would reduce this amount. If there was less pore ice, ~10% as was hypothesized at Hale crater (Jones et al., 2011), melting as described would yield sufficient water to fill the upper basin by a factor of 1.5X. By contrast, greater ice porosity (up to 50%, Squyres et al., 1992) or melting to greater depth beneath the ejecta would increase the amount of available water (though models for post-hydrothermal systems suggest freezing at and outside the rim is geologically rapid, see Barnhart et al., 2010). Hence, sufficient ground ice may have been accommodated and available in the pre-impact region to account for the water necessary for forming the relatively pristine valleys. Additional inventories, in the form of a pre-existing snow or ice pack on the surface, were probably not required.

In contrast to Hale and Lyot, the relatively pristine valleys occur only on the west side of Jones crater. And there are other features seen around Hale and Lyot craters that do not occur around Jones, such as lobate deposits at the end of valleys that are capped by transverse ridges and digitate terminus and the more subtle, fluidized distal ejecta features. We now explore whether the differences between the relatively pristine drainage features at Jones and around Hale and Lyot craters can be accommodated in a model involving formation during post-impact discharge sourced by melting ice and (or) water in and below the Jones crater ejecta shortly after formation of the crater.

The occurrence of relatively pristine valleys on only the west side of Jones crater could relate to the influence of regional topography on drainage. The impact that formed Jones crater occurred on the lower east flank of the Chryse trough and into relief associated with one of the outer rings of Ladon basin (**Figs. 1 and 3**). As a result, the crater and its surrounding ejecta are generally tilted towards the west-northwest, with a distinct lower trough west of the crater being created where topography of the Ladon basin ring descends into the axis of the Chryse trough (**Figs. 1 and 3**). Unlike at Hale crater, most water melted by the impact in and below the ejecta would not have drained radially away from all sides of the crater. Drainage away from the crater on and within ejecta to the east, north and south would have been limited and likely have precluded appreciable valley incision. Instead, the general flat to west-northwest tilt of the surface coupled with the likely high infiltration capacity and permeability of the ejecta means most impact melted ice/water on the east, and perhaps north, and south sides of the crater would drain into the subsurface with some possibly flowing west and increasing the inventory of water on the western side of the crater. Because the few potentially significant tributaries to the relatively pristine valley segments occur on the steeper, western flank of Jones (**Fig. 3**) where sufficiently steep slopes may have enabled some runoff, most water may have drained in the warmer subsurface. Regardless, water on the surface and subsurface would have eventually emerged at the base of the topographic trough on the west side of Jones, accumulating in the upper and lower basins before eventually breaching their divides and discharging northward and then along the trough axis (**Fig. 3**).

Although there is an absence of lobate deposits outside of Jones that are equivalent to the transverse ridge-topped and digitate-ended features at Hale crater, there is a deposit on the floor of Jones crater that may be analogous or could be a deposit of impact melt (**Fig. 20**). There are no obvious associated volcanic vents or deposits visible within Jones, but it is possible one could be buried by alluvium transported and emplaced in fans emanating from the northeast and east side of the crater wall. Nevertheless, the absence of such features outside the crater could relate to a greater role played by groundwater drainage in the delivery and accumulation of water on the west side of the crater and that would have reduced the time necessary for filling the basins. The topography on the ejecta west of Jones may have precluded formation of lobate deposits by enabling efficient accumulation of water in the basins that was then able to drain northward unimpeded, perhaps at least partially along the pre-impact course of Samara Valles. It is possible that the rate at which impact melted water was made available southwest of Jones was relatively less than at Hale and Lyot and limited the transport of high sediment loads forming such deposits. Relatively lower or slower discharge of water sourcing the upper and lower basins over a shorter period at Jones is also consistent with a single, brief drainage event as is hypothesized. Finally, there are not clear analogs around Jones for the fluidized distal ejecta features observed around Hale, though it is possible that the flat-topped features ~100 km south of Jones (**Fig. 7**) are the result of limited and local melting and flow related to their emplacement. More likely, however, we suspect that the subtle appearance of these localized and thin deposits around the younger Hale crater suggests their recognition could easily be precluded by even a small amount of degradation had they been present around Jones. That would be consistent with the greater age and longer history of erosion at Jones and evidence that even the relatively pristine valley segments have experienced local infilling and some modification.

The fairly isolated origination of the relatively pristine valleys mostly or entirely on the Jones ejecta deposit that were active over a geologically brief period, well below the crater rim, and only on the west side of the crater argues strongly against a regional or global climatic trigger for formation. Evidence of a longer duration of discharge and more uniform and (or) regional origin and distribution of relatively pristine valley segments on and beyond the Jones ejecta as well as reactivation of valley segments further to the south would be expected if drainage were climate driven. Alluvial fans are observed along some or all of the walls in a number of craters across the southern Margaritifer Terra region and their formation may have been climate driven (Grant and Wilson, 2011; 2012). In Jones crater, the best developed alluvial fans occur on the northeast and eastern rim and interior walls and they are largely absent from the western wall (**Fig. 2**; Mangold et al., 2012). In addition, valleys sourcing the larger Jones fans originate in alcoves high on the crater wall, are much smaller, better preserved, and likely younger (Grant and Wilson, 2011) than the relatively pristine segments along Samara Valles based on the scale of fine scale morphology visible on the fans. Finally, the location of the fans within Jones crater presents no obvious tributary or other connection to activity occurring along the relatively pristine segments on much lower surfaces well outside the west side of the crater.

We believe that the extent, morphometry, and distribution of the relatively pristine Samara Valles segments is most consistent with an origin related to the Jones impact event. The unique topographic setting and factors potentially including excavation and melting of sufficient ice at Jones, combined with some, but limited erosion since the Late Hesperian, can account for the distribution of relatively pristine valleys at Jones and the absence of some other landforms observed at Hale crater. We propose that formation of Jones crater was followed by westward, surface, and perhaps even more significant subsurface, drainage of water melted by the impact that filled at least the upper basin over a period of months to perhaps decades. The more important groundwater was to basin infilling, the shorter the period of basin filling may have been. However, once the upper basin overtopped the divide on the northeast side, much of the water drained rapidly over a period likely not exceeding years.

At least some of the thicker continuous ejecta around Jones may have remained relatively warm for hundreds of years (Mangold, 2012), but the thinner distal and other near-surface portions of the deposit (to depths of meters) would have cooled more quickly if climate during the Late Hesperian was cold and dry and similar to the present (e.g., Warner et al., 2010), thereby leading to the possibility of an ice cover on the flooded basins. There is little unique evidence, however, for or against existence of an ice cover on water ponded in the basins or along the relatively pristine valleys themselves that might help constrain global conditions. For example, benches near the divide in the upper basin could have been eroded by either wave action or ice push grinding along the margin of flooding. In addition, valley incision could have been assisted by blocks of ice grinding along the valley sides during discharge (e.g., Beltaos and Burrell, 2021), but is not required.

As water drained out of the upper basin and incised northward along the trough axis, perhaps at least partially along the pre-impact course of Samara Valles, it created a series of terraces and depositional features that remain visible today. The flowing water quickly overwhelmed the smaller lower basin and breached the downstream divide as well as additional local divides before becoming less confined, less incised, and expanding into the trough further north to create a series of layered deposits. Drainage into the upper basin and further downstream effectively ceased about the time drainage from the upper basin ended. The ultimate fate of the water and whether it reached Margaritifer basin is unknown and perhaps obscured by degradation associated with even later volcanic activity at the downstream end of the system (Wilson et al., 2022).

We interpret the relatively pristine valley segments along Samara Valles and west of Jones crater as an example of discharge and valley formation and (or) reactivation associated with a large impact event that is broadly analogous to what has been documented around the younger Hale and other craters (Dickson et al., 2009; Jones et al., 2011; El-Maarry et al., 2013, Grant and Wilson, 2017; Weiss et al., 2017). If our model is correct, then late water activity and high discharge along the relatively pristine Samara Valles segments occurred over a geologically brief interval (months to years) and was unrelated to global climate. Nevertheless, and regardless of whether climate was relatively warm or cold at the time, the formation of surface water reservoirs and active fluvial processes west of Jones likely created transient habitable environments relatively late in Martian history.

Acknowledgements and Data:

We thank Alan Howard, Alex Morgan, and the editors of the MRO special issue for comments and suggestions that improved the manuscript. Many thanks also to Pebbles. This work was supported by grant 80NSSC20K0551 to S. Wilson (includes J. Grant as Co-I) from the National Aeronautics and Space Administration and a Smithsonian Institution NASM Summer Internship (to R. Manogaran). All data used in the paper is freely accessible at the PDS and(or) websites for HiRISE (https://www.uahirise.org/hiwish/browse), CTX (http://global-data.mars.asu.edu/bin/ctx.pl), MOLA (https://pds-geosciences.wustl.edu/missions/mgs/mola.html), and CRISM (http://crism-map.jhuapl.edu/) data websites, and(or) at Smithsonian.figshare: https://doi.org/10.25573/data.24153258.

References:

Alemanno, G., Orofino, V., and Mancarella, F., 2018. Global Map of Martian fluvial systems: Age and total eroded volume estimates: Earth and Space Science, 10, 560-577, 10.1029/2018EA000362.

Baker, V. R., The Channels of Mars, 198 pp., Univ. Texas Press, Austin, 1982.

Baker, V. R., and Partridge, J. B., 1986. Small Martian valleys: Pristine and degraded morphology: Journal of Geophysical Research, 91, B3, 3561-3572.

Baker, V. R., Carr, M. H., Gulick, V. C., Williams, C. R., and Marley, M. S., Channels and valley networks, in Mars, edited by H. H. Kieffer et al., p. 493-522, Univ. Arizona Press, Tucson, AZ, 1992.

Banerdt, W. B., 2000. Surface drainage patterns on Mars from MOLA topography: Eos Trans. AGU, 81(48), Fall Meet. Suppl., P52C-04.

Beltaos, S., and Burrell, B. C., 2021. Effects of river-ice breakup on sediment transport and implications to stream environments: A review: Water, 13 (18), 2541, 10.3390/w13182541.

Brown, W. K. (1989). A theory of sequential fragmentation and its astronomical applications. Journal of Astrophysics and Astronomy, 10, 89-112.

Burr, D. M., Williams, R. M. E., Wendell, K. D., Chojnacki, M., Emery J. P., 2010. Inverted fluvial features in the Aeolis/Zephyria Plana region, Mars: formation mechanism and initial paleodischarge estimates: Journal of Geophysical Research, 115 (E7), E07011, 10.1029/2009JE003496

Carr, M. H., 1995. The Martian drainage system and the origin of valley networks and fretted channels: Journal of Geophysical Research, 100 (E4), 7479–7507, 10.1029/95JE00260

Carr, M. H., Water on Mars. Oxford University Press, New York, 1996.

Carr, M. H., The surface of Mars, Cambridge Planetary Science Series. Cambridge Univ. Press, Cambridge, 2006.

Carr, M. H., and Chuang, F. C., 1997. Martian drainage densities: Journal of Geophysical Research, 102(E4), 9145–9152, 10.1029/97JE00113.

Christensen, P. R. et al., 2001. Mars Global Surveyor Thermal Emission Spectrometer experiment: Investigation description and surface science results: Journal of Geophysical Research, 106, E10, 23823-23871.

Dickson, J. L., Fassett, C. I., Head, J. W., 2009. Amazonian-aged fluvial valley systems in a climatic microenvironment on Mars: Melting of ice deposits on the interior of Lyot Crater: Geophysical Research Letters, 36 (8): L08201, 10.1029/2009GL037472.

Dickson, J. L., Kerber, L. A., Fassett, C. I, and Ehlmann, B. L., 2018. A global, blended CTX mosaic of Mars with vectorized seam mapping: A new mosaicking pipeline using principles of non-destructive image editing: Lunar and Planetary Science Conference, XLIX: Houston, Tex., Lunar and Planetary Institute, Abstract #2480.

Edwards, C. S., Nowicki, K. J., Christensen, P. R., Hill, J., Gorelick, N., and Murray, K., 2011. Mosaicking of global planetary image datasets: 1. Techniques and data processing for Thermal Emission Imaging System (THEMIS) multi-spectral data: Journal of Geophysical Research, 116, E10008, 10.1029/2010JE003755.

El-Maarry M. R., Dohm J. M., Michael G., Thomas N., and Maruyama S., 2013. Morphology and evolution of the ejecta of Hale crater in Argyre basin, Mars: Results from high resolution mapping: Icarus, 226: 905– 922, 10.1016/j.icarus.2013.07.014.

Fassett, C. I., and Head, J. W., III, 2008. The timing of Martian valley network activity: Constraints from buffered crater counting: Icarus, 195, 61-89, 10.1016/j.icarus.2007.12.009.

Folk, Robert L. Petrology of Sedimentary Rocks. Austin, Tex: Hemphill Pub. Co, 1980.

Frey, H. V., 2008. Ages of very large impact basins on Mars: Implications for the late heavy bombardment in the inner solar system: Geophysical Research Letters, 35, 10.1029/2008GL033515.

Glotch, T. D., Bandfield, J. L., Wolff, M. J., Arnold, J. A., and Che, C., 2016. Constraints on the composition and particle size of chloride salt-bearing deposits on Mars: Journal of Geophysical Research, 121(3), 454–471, 10.1002/2015je004921.

Grant, J. A., 1987. The geomorphic evolution of Eastern Margaritifer Sinus, Mars: Advances in planetary geology, NASA Technical Memorandum 89871, p. 1-268.

Grant, J. A., 2000. Valley formation in Margaritifer Sinus, Mars, by precipitation-recharged ground-water sapping: Geology, 28, 223-226.

Grant, J.A., and P. H. Schultz (1993), Degradation of selected terrestrial and Martian impact craters: *J. Geophys. Res.*, 98, 11,025-11,042, 10.1029/93JE00121

Grant, J. A., and Parker, T. J., 2002. Drainage Evolution of the Margaritifer Sinus Region, Mars: Journal of Geophysical Research, 107, 10.1029/2001JE001678.

Grant, J., and Fortezzo, C., 2003. Basin hypsometry on the Earth, Mars, and the Moon: 6th Mars Conference Abstracts, July 21-25, 2003, Caltech, Pasadena, CA.

Grant, J. A., and Wilson, S A., 2017. The nature and emplacement of distal aqueous-rich ejecta deposits from Hale crater, Mars: Meteoritics and Planetary Science, 53, 10.1111/maps.12843.

Grant, J. A., Wilson, S. A., Fortezzo, C. M., and Clark, D. A., 2009. Geologic map of MTM -20012 and -25012 quadrangles, Margaritifer Terra region of Mars: U.S. Geological Survey, Scientific Investigations Map 3041, scale 1:500,000.

Grant, J. A., Manogaran, R., and Wilson, S. A., 2023. Data Repository for Late Drainage Along Portions of Samara Valles, West of Jones Crater, Margaritifer Terra, Mars: Smithsonian figshare. https://doi.org/10.25573/data.24153258.

Hynek, B. M., 2015. Valley networks and the nature of the Late Noachian Mars climate: LPSC XLVI, abstract 2166, LPI, Houston, TX.

Hynek, B. M., Beach, M., and Koke, M. R. T., 2010. Updated global map of Martian valley networks and implications for climate and hydrologic processes: Journal of Geophysical Research, 115, 10.1029/2009JE003548.

Irwin, R. P., III, and Grant, J. A., 2013. Geologic Map of MTM –15027, –20027, –25027, and –25032 Quadrangles, Margaritifer Terra Region of Mars: U.S. Geological Survey, Scientific Investigations Map 3209, Scale 1:1,000,000.

Jacobsen, R. E., and Burr, D. E., 2018. Errors in Martian paleodischarges skew interpretations of hydrologic history: Case study of the Aeolis Dorsa, Mars, with insights from the Quinn River, NV: Icarus, 302, 407-417, 10.1016/j.icarus.2017.11.014.

Jones, A. P., McEwen A. S., Tornabene L. L., Baker V. R., Melosh H. J., and Berman D. C., 2011. A geomorphic analysis of Hale crater, Mars: The effects of impact into ice-rich crust: Icarus, 211: 259–272, 10.1016/j.icarus.2010.10.014.

Kleinhans, M. G., 2005. Flow discharge and sediment transport models for estimating a minimum timescale of hydrological activity and channel and delta formation on Mars: Journal of Geophysical Research, 110, (E12003), 10.1029/2005JE002521.

Konsoer, K. M., LeRoy, J., Burr, D., Parker, G., Jacobsen, R., and Turmel, D., 2018. Channel slope adjustment in reduced gravity environments and implications for Martian channels: Geology, 46 (2), 183-186, 10.1130/G39666.1.

Leask, E. K., and Ehlmann, B. L., 2022. Evidence for deposition of chloride on Mars from small-volume surface water events into the Late Hesperian-Early Amazonian: AGU Advances, 3, e2021AV000534, 10.1029/2021AV000534.

Malin, M. C., et al., 2007. Context Camera Investigation on board the Mars Reconnaissance Orbiter: Journal of Geophysical Research, 112, E05S04, 10.1029/2006JE002808.

Mangold, N., 2012. Fluvial landforms on fresh impact ejecta on Mars: Planetary and Space Science, 62 (1), 69-85, 10.1016/j.pss.2011.12.009.

Mangold, N., Adeli, S., Conway, S., Ansan, V., and Langlais, B., 2012. A chronology of early Mars climatic evolution from impact crater degradation: Journal of Geophysical Research, 117, E04003, 10.1029/2011JE004005.

Mangold, Gupta, S., Gasnault, O, Dromart, G., Tarnas, J. D., Sholes, S. F., et al., 2021, Perseverance rover reveals an ancient delta-lake system and flood deposits at Jezero crater, Mars. Science, 374, 711-717. 10.1126/science.abl4051.

McEwen, A. S., et al., 2007. Mars Reconnaissance Orbiter's High Resolution Imaging Science Experiment (HiRISE): Journal of Geophysical Research, 112, E05S02, 10.1029/2005JE002605.

Melosh, H. J., 1989, Impact Cratering, 245 pp., Oxford University Press, New York.

Murchie, S., R. Arvidson, P. Bedini, K. Beisser, J.-P. Bibring, J. Bishop, J., Boldt, P. et al., 2007. Compact Reconnaissance Imaging Spectrometer for Mars (CRISM) on Mars Reconnaissance Orbiter (MRO): Journal of Geophysical Research, 112, E05S03, 10.1029/2006JE002682.

Osterloo, M., Hamilton, V., Bandfield, J., Glotch, T., Baldridge, A., Christensen, P., et al., 2008. Chloride-bearing materials in the southern highlands of Mars: Science, 319 (5870), 1651–1654, 10.1126/science.1150690.

Osterloo, M. M., Anderson, F. S., Hamilton, V. E., and Hynek, B. M., 2010. Geologic context of proposed chloride-bearing materials on Mars: Journal of Geophysical Research, 115(E10), E10012, 10.1029/2010je003613.

Parker, T. J., 1985. Geomorphology and Geology of the Southwestern Margaritifer Sinus-Northern Argyre Region of Mars: Master’s Thesis, California State Univ., LA.

Phillips, R. J., Zuber, M. T., Solomon, S. C., Golombek, M. P., Jakosky, B. M., Banerdt, W. B., Smith, D.E., Williams, R. M. E., Hynek, B. M., Aharonson, O., and Hauck, S. A., II, 2001. Ancient geodynamics and global-scale hydrology on Mars: Science, 291, 2587-2591.

Rotto, S., and K. L. Tanaka, 1995. Geologic/geomorphic map of the Chryse Planitia region of Mars: U.S. Geological Survey Miscellaneous Investigations Series Map I-2441, Scale: 1:X.

Salvatore, M. R., Kraft, M. D., Edwards, C. S., and Christensen, P. R., 2016. The geologic history of Margaritifer basin: Journal of Geophysical Research, 121, 273-295, 10.1002/2015JE004938.

Saunders, S. R., 1979. Geologic map of the Margaritifer Sinus Quadrangle of Mars: U.S. Geological Survey Mars Map Series I-1144, quadrangle MC-19, scale 1:5 000 000.

Schultz, P. H., and Glicken, H., 1979. Impact crater and basin control of igneous processes on Mars: Journal of Geophysical Research, 84, 8033–8047.

Schultz, P. H., Schultz, R. A. and Rogers, J., 1982. The structure and evolution of ancient impact basins on Mars: Journal of Geophysical Research, 87, 9803-9820.

Smith, D. E., Zuber, M. T., Frey, H. V., et al., 2001. Mars Orbiter Laser Altimeter—Experiment summary after the first year of global mapping of Mars: Journal of Geophysical Research, 106, E10, 23,689–23,722.

Squyres, S. W., Clifford, S. M., Kuzmin, R. O., Zimbelman, J. R., and Costard, F. M., 1992. Ice in the Martian regolith, Chapter 16, p. 523-554 *in* H. H. Kieffer, B. M. Jakosky, C. W. Snyder, and M. S. Matthews (eds.): Mars. The University of Arizona Press, Tucson/London

Tanaka, K., Skinner, J. A., Jr., Dohm, J. M., Irwin, R. P., III, Kolb, E. J., Fortezzo, C. M., Platz, T., et al., 2014. Geologic map of Mars: U. S. Geological Survey Sci. Invest., Map 3292, Scale: 1:20,000,000.

Warner, N., Gupta, S., Lin, S-Y., Kim, J-R., Muller, J-P., and Morley, J., 2010. Late Noachian to Hesperian climate change on Mars: Evidence of episodic warming from transient lakes near Ares Vallis: Journal of Geophysical Research, 115 (E6), 10.1029/2009JE003522.

Weiss, D. K., Head, J. W., Palumbo, A. M., and Cassanellis, J. P., 2017. Extensive Amazonian-aged fluvial channels on Mars: Evaluating the role of Lyot crater in their formation: Journal of Geophysical Research, 44, 5336-5344, 10.1002/2017GL073821.

Weitz, C. M., Wilson, S. A., Grant, J. A., and Irwin, R. P., III, 2023. Geologic map of western Ladon basin, Mars, MTM Quadrangles, -15032 and -20032: USGS Scientific Investigation Map, scale 1:1,000,000, scale 1:1:000,000, in press.

Wilson, L., Ghatan, G. J., Head, J. W., and Mitchell K. L., 2004. Mars outflow channels: A reappraisal of the estimation of water flow velocities from water depths, regional slopes, and channel floor properties: Journal of Geophysical Research, 109, E09003, 10.1029/2004JE002281.

Wilson, S. A., and Grant, J. A., 2018. Alluvial fans in Roddy crater on Mars: Planetary Geologic Mappers Meeting Abstract, June, 12-14, Knoxville, TN.

Wilson, S. A., Grant, J. A., Williams, K. K., 2022. Geologic map of Morava Valles and Margaritifer basin, Mars, MTM Quadrangles -10022 and -15022: U. S. Geological Survey Scientific Investigation Map 3489, scale 1:1,000,000.

Wilson, S. A., and Grant, J. A., 2023, Geologic mapping of MTM quadrangles -20022, -25022, -20017, and -25017 in Margaritifer Terra on Mars: Geol. Soc. America Abs. with Programs, abstract 394640.

Table 1: Summary of Parameters Used in Discharge Estimates (discharge estimates expressed in units of 10^4 m^3s^{-1}, see also Supplementary Data File).

Profile Number **(Figure 4)**	Channel Width Profile (m)	Average Channel Depth (m)	Gradient Measured Along the Channel	Average Discharge for Rectangular Cross Section (Wilson et al., 2004)	Average Discharge for Rectangular Cross Section (Mangold et al., 2021)	Average Discharge for Triangular Cross Section (Wilson et al., 2004)	Average Discharge for Triangular Cross Section (Mangold et al., 2021)
Profile 1	586	10	$5.0 X 10^{-4}$	$1.1 X 10^{4} m^{3}s^{-1}$	$1.0 X 10^{4} m^{3}s^{-1}$	$0.4 X 10^{4} m^{3}s^{-1}$	$0.3 X 10^{4} m^{3}s^{-1}$
Profile 2	201	11	$5.0 X 10^{-4}$	$0.4 X 10^{4} m^{3}s^{-1}$	$0.4 X 10^{4} m^{3}s^{-1}$	$0.1 X 10^{4} m^{3}s^{-1}$	$0.1 X 10^{4} m^{3}s^{-1}$
Profile 3	840	72	$4.2 x 10^{-3}$	$91 X 10^{4} m^{3}s^{-1}$	$85 X 10^{4} m^{3}s^{-1}$	$30 X 10^{4} m^{3}s^{-1}$	$28 X 10^{4} m^{3}s^{-1}$
Profile 4	909	19	$3.2 x 10^{-3}$	$11 X 10^{4} m^{3}s^{-1}$	$10 X 10^{4} m^{3}s^{-1}$	$3.6 X 10^{4} m^{3}s^{-1}$	$3.3 X 10^{4} m^{3}s^{-1}$
Profile 5	772	20	$3.2 x 10^{-3}$	$10 X 10^{4} m^{3}s^{-1}$	$9.4 X 10^{4} m^{3}s^{-1}$	$3.3 X 10^{4} m^{3}s^{-1}$	$3.1 X 10^{4} m^{3}s^{-1}$
Profile 6	750	32	$3.2 x 10^{-3}$	$20 X 10^{4} m^{3}s^{-1}$	$19 X 10^{4} m^{3}s^{-1}$	$6.7 X 10^{4} m^{3}s^{-1}$	$6.3 X 10^{4} m^{3}s^{-1}$
Profile 7	620	11	$4.0 x 10^{-3}$	$3.4 X 10^{4} m^{3}s^{-1}$	$3.2 X 10^{4} m^{3}s^{-1}$	$1.1 X 10^{4} m^{3}s^{-1}$	$1.0 X 10^{4} m^{3}s^{-1}$
Profile 8	620	15	$4.0 x 10^{-3}$	$5.6 X 10^{4} m^{3}s^{-1}$	$5.2 X 10^{4} m^{3}s^{-1}$	$1.8 X 10^{4} m^{3}s^{-1}$	$1.7 X 10^{4} m^{3}s^{-1}$

Figures And Captions:

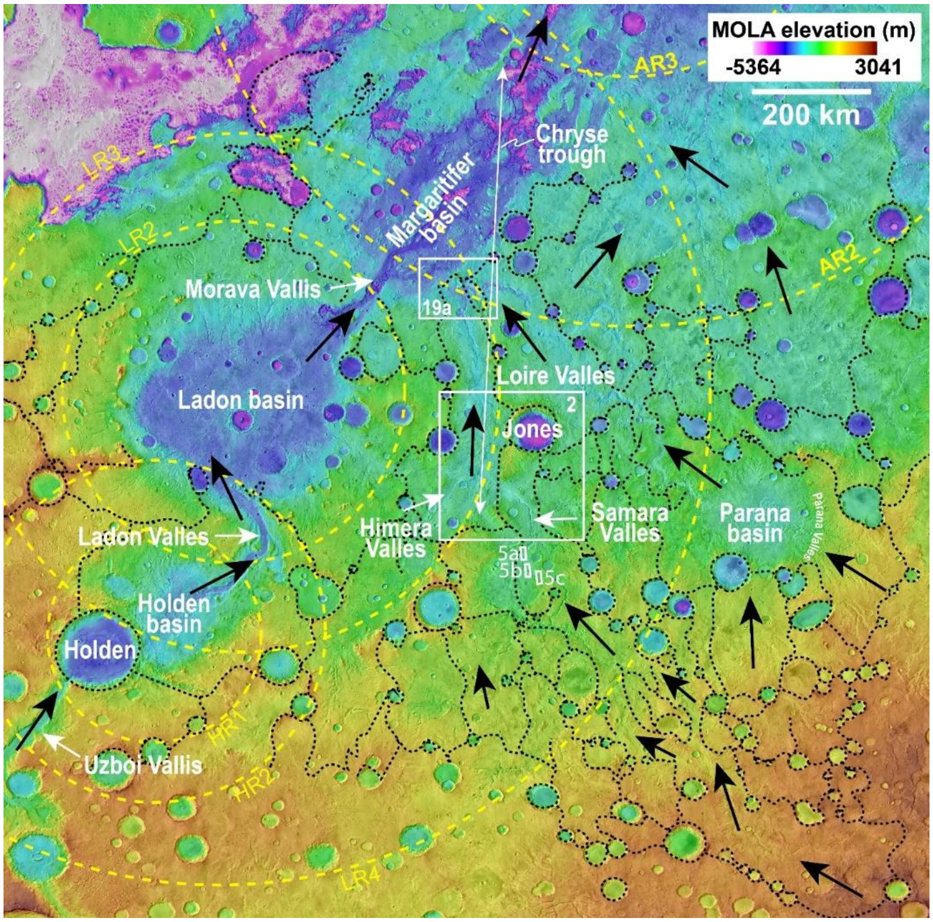

Figure 1. Margaritifer Terra region with major placenames (area covers 5°S to 35°S and between ~325°E to 350°E). Drainage basin boundaries (dashed black, see Grant (1987; 2000) and Grant and Parker (2002)) and routed flow (black arrows) were influenced by remnant topography of the Chryse trough (axis white double arrow) and ancient multi-ringed impact basins (yellow dashed lines, Schultz et al., 1982) that are indicated for Holden (Holden rings (HR) 1 and 2 (HR1 and HR2, respectively), Ladon rings (LR) 2-4 (LR2, LR3, and LR4, respectively), and Ares rings (AR) 2 and 3 (AR2 and AR3, respectively)). Boxes indicate location of Figures 2, 5a, 5b, 5c, and 19a. Location of remaining Figures indicated on Figures 2 (except for Figure 14 which is indicated on Figure 19a). MOLA (Smith et al., 2001) color elevation over THEMIS daytime IR (Christensen et al., 2001; Edwards et al., 2011). North to top.

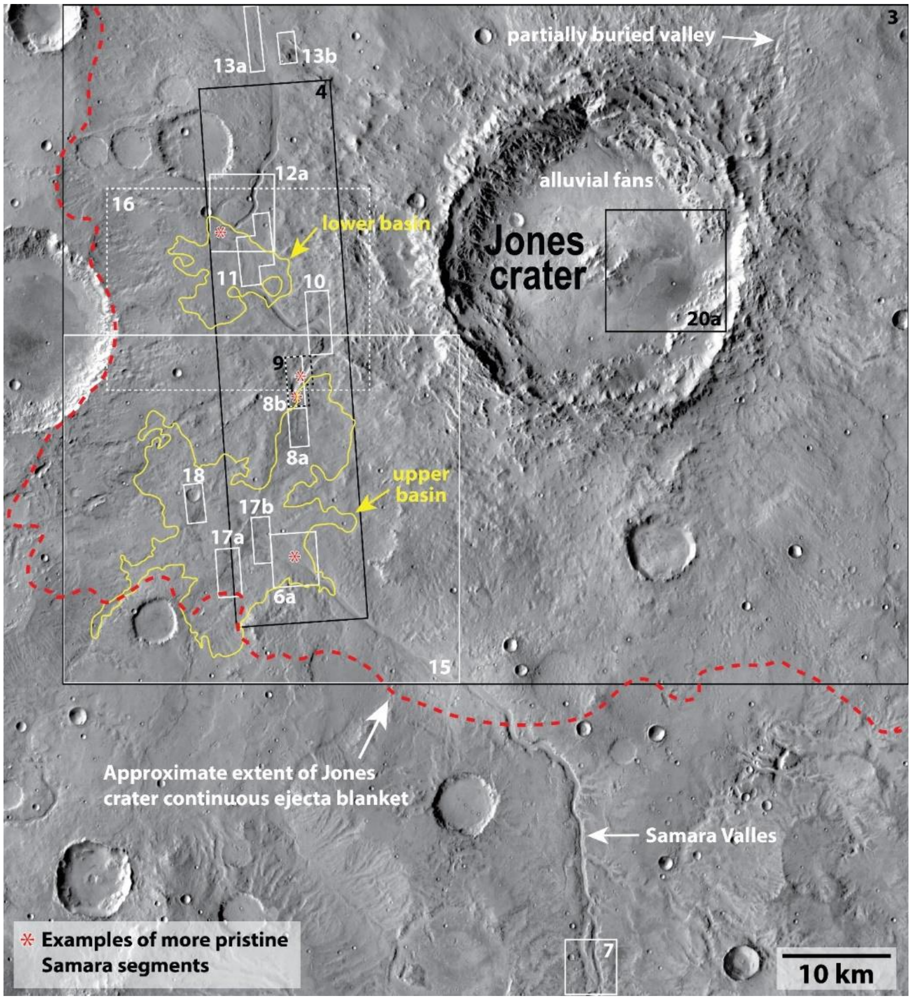

Figure 2. Jones crater and region to the west incised by relatively pristine valleys approximately 17.5°S to 22°S and between 337°E to 342.5°E (see Figure 1 for context). Valleys traversing to the west of the crater incise the ejecta (approximate extent indicated by red dashed line) surrounding Jones crater and appear relatively pristine (example locations shown by "*"). By contrast, a valley to the northeast of Jones is more degraded and appears partially buried by Jones ejecta. Only rare examples of other possible surface drainages are present, with perhaps the best candidate being located at and below the southwest corner of Jones. Approximate areal extent of upper and lower basins indicated (yellow lines). Boxes indicate location of Figures 3, 4, 6-13, 15-18, and 20a. Mosaic of CTX images with original resolution of ~6 m/pixel that has been reprocessed to 1200 dpi for mapping. North is towards the top.

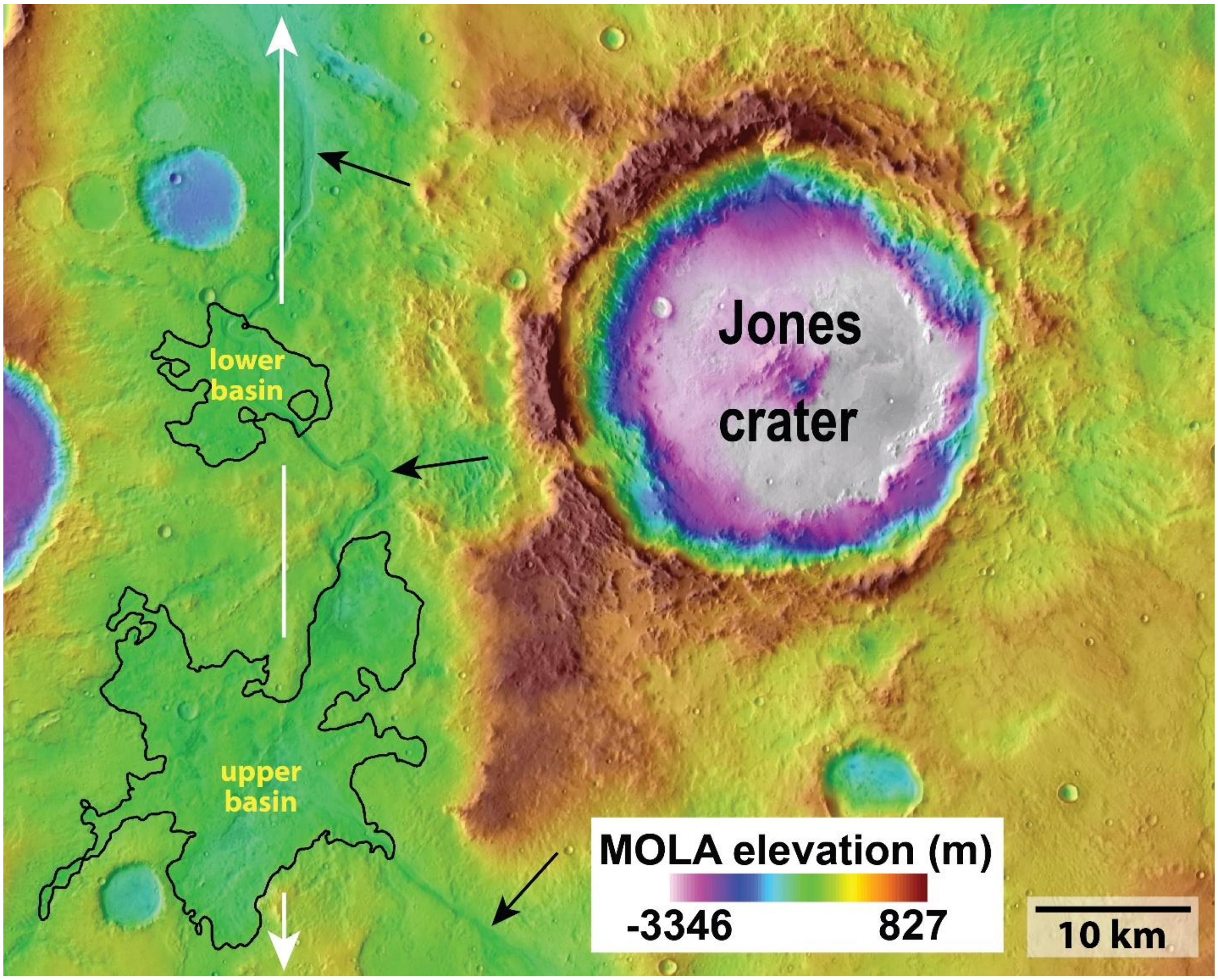

Figure 3. Jones crater impacted along the margin of the north-south trending Chryse trough (white line with double headed arrows) and between outer rings of Ladon basin (see Figure 2 for context). The topography associated with the Jones crater rim is quite pronounced and rugged. Relatively pristine segments of Samara Valles (black arrows) traverse the ejecta west of Jones crater along the floor of the Chryse trough as the system drains to the north (top of the image). Approximate areal extent of upper (Fig. 15) and lower (Fig. 16) basins indicated (black lines). MOLA data (128 pixels/degree, ~463 meter per pixel in N-S direction) over THEMIS daytime IR (100 meter per pixel mosaic) (Christensen et al., 2001; Edwards et al., 2011). North is towards the top.

953

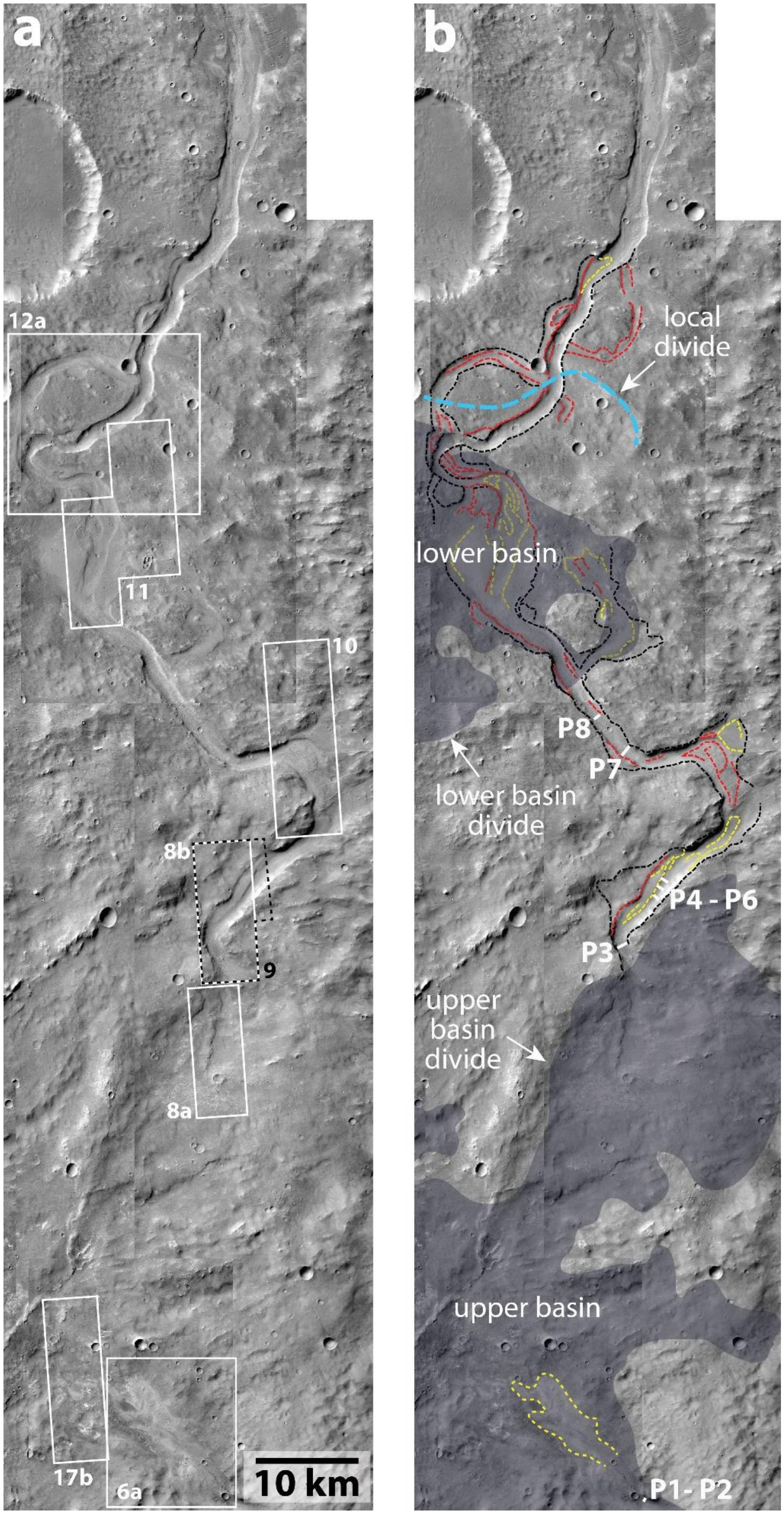
a
12a
11
10
8b
9
8a
17b
6a
10 km
b
local
divide
lower basin
P8
P7
lower basin
divide
P4 - P6
P3
upper
basin
divide
upper basin
P1- P2

Figure 4. **a**) Relatively pristine segments of Samara Valles west of Jones crater incise the Jones ejecta (see Fig. 2 for context). A smaller, upstream valley segment is bounded by lobate deposits where it enters the upper basin (dashed yellow line near bottom of 4b). Segments emerging downstream of the upper basin are larger, continue through a smaller, lower basin and beyond the Jones ejecta. Boxes indicate location of Figures 6a, 8-12 and 17b. **b**) Red and yellow dotted lines in denote terraces and deposits, respectively. Shaded areas represent the maximum extent (correlating to the -1275 m MOLA contour) of the upper and lower basins (see Figs 15-16). Drainage divides associated with the upper and lower basin as well as local divides (e.g., blue dashed line) influenced the flow of water across the landscape. White lines mark locations of 8 profiles (P1-P8) that correspond to idealized cross sections used to estimate discharge (P1 and P2 shown as single line due to close proximity). For both panels, CTX mosaic covers 15.1°S to 17.4°S between 330.9°E to 332.7°E. CTX images available at: http://global-data.mars.asu.edu/bin/ctx.pl with original resolution of ~6 m/pixel. Downstream is from the bottom to the top of the image. North is toward the top.

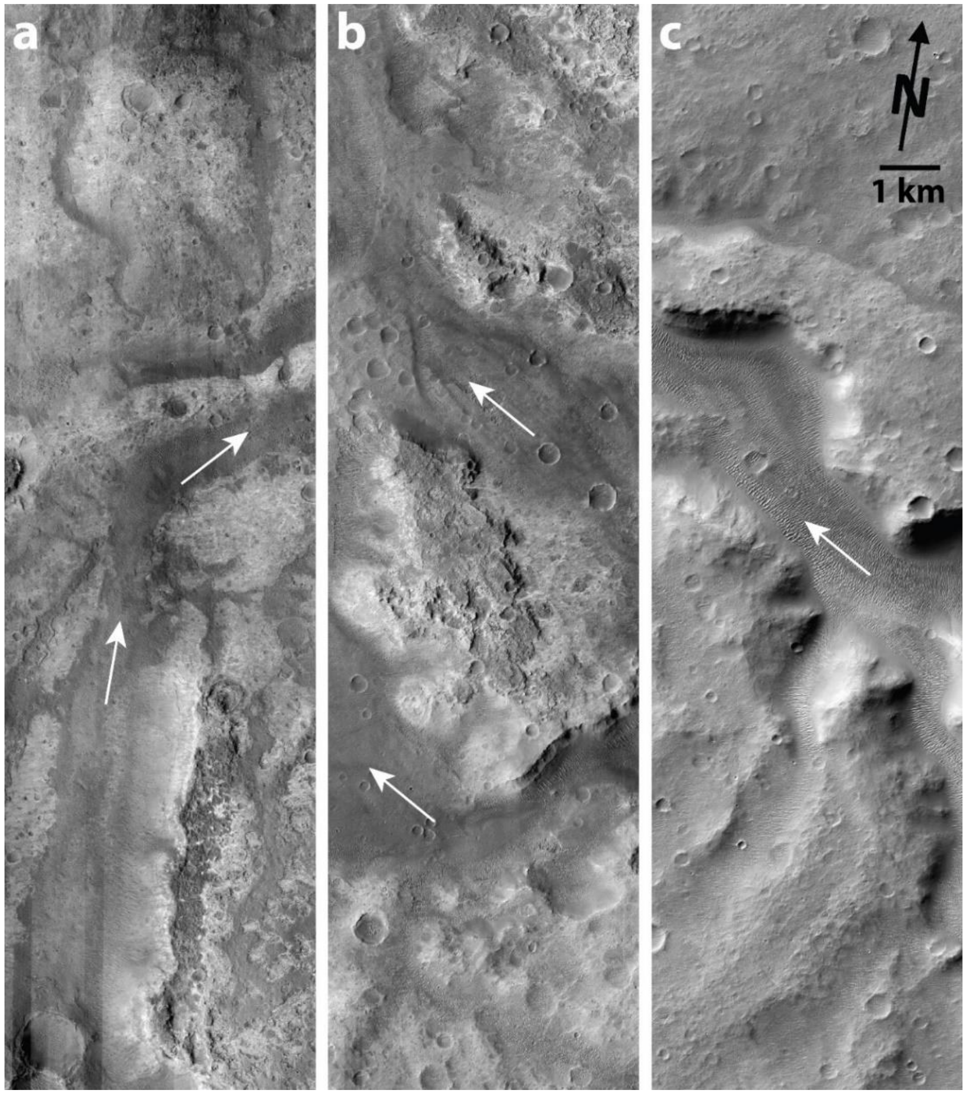

Figure 5. Degraded appearance of upstream segments of Samara Valles (see Figure 1 for context). These three examples of Samara Valles are within ~100 km of one another and are located beyond the southern extent of the Jones continuous crater ejecta. Note typically irregular and (or) sometimes poor definition of valley sides and covered appearance of the floor in **a-c**. The degraded nature of the valley here is typical of the appearance of the valley south and upstream of the limit of the continuous ejecta deposit of Jones crater. White arrows show downstream direction. HiRISE images (0.5 m-pixel scale) **a**) ESP_074219_1570_RED, **b**) ESP_073441_1565_RED, and **c**) ESP_026943_1560_RED.

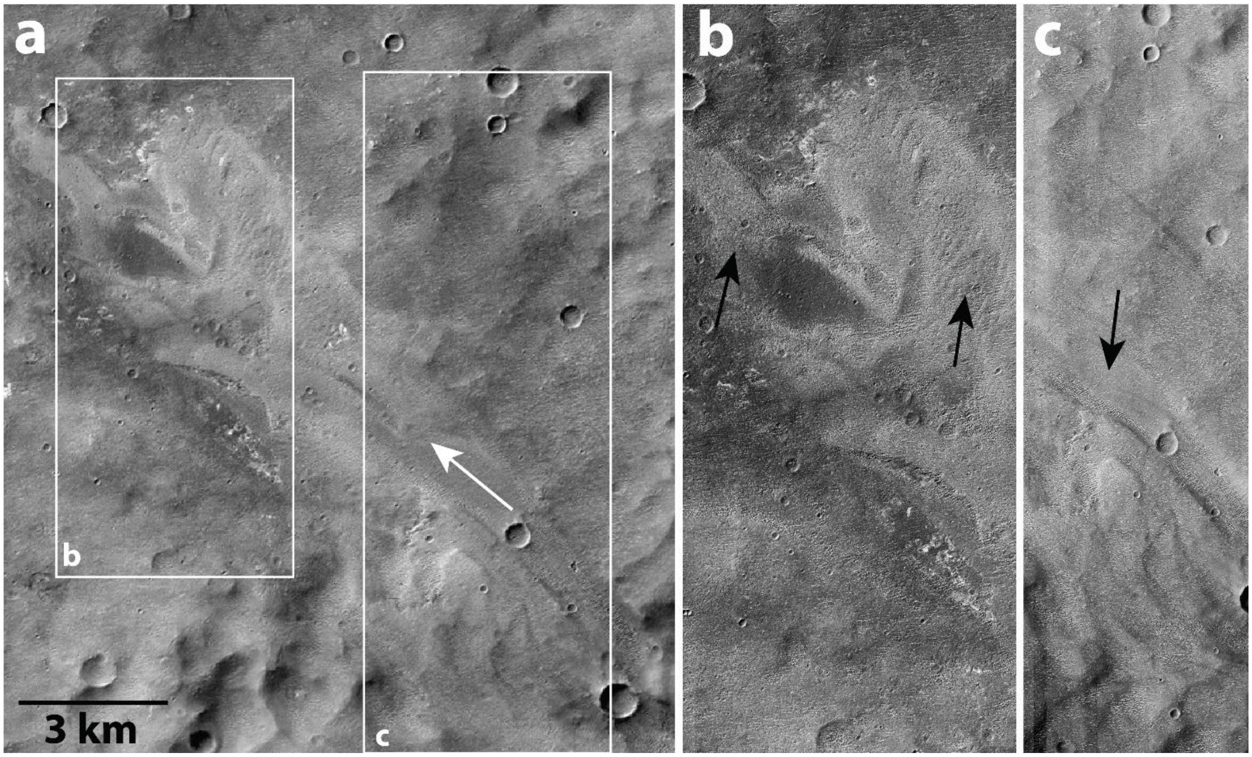

Figure 6. a) The appearance of Samara Valles changes near the margin of the Jones crater ejecta deposit (see Figures 2 and 4 for context) and takes on a relatively pristine expression compared to the valley further south (**Fig. 5**). The initially small and shallow relatively pristine valley incises Jones ejecta southwest of the crater and is characterized by a series of splaying or lobate, likely depositional forms that include steep-fronted examples at an elevation close to -1275 m MOLA (Smith et al., 2001) (see Fig. 4 for context). White arrow indicates downstream direction. CTX image D17_033734_1595_XN_20S021W (5.16 m-pixel scale). **b**) Black arrows indicate examples of late deposits as seen in HiRISE image ESP_033734_1595_RED (0.50 m-pixel scale). **c**) Black arrows indicate examples of late deposits as seen in HiRISE image ESP_073085_1595_RED (0.50 m-pixel scale). North is toward the top.

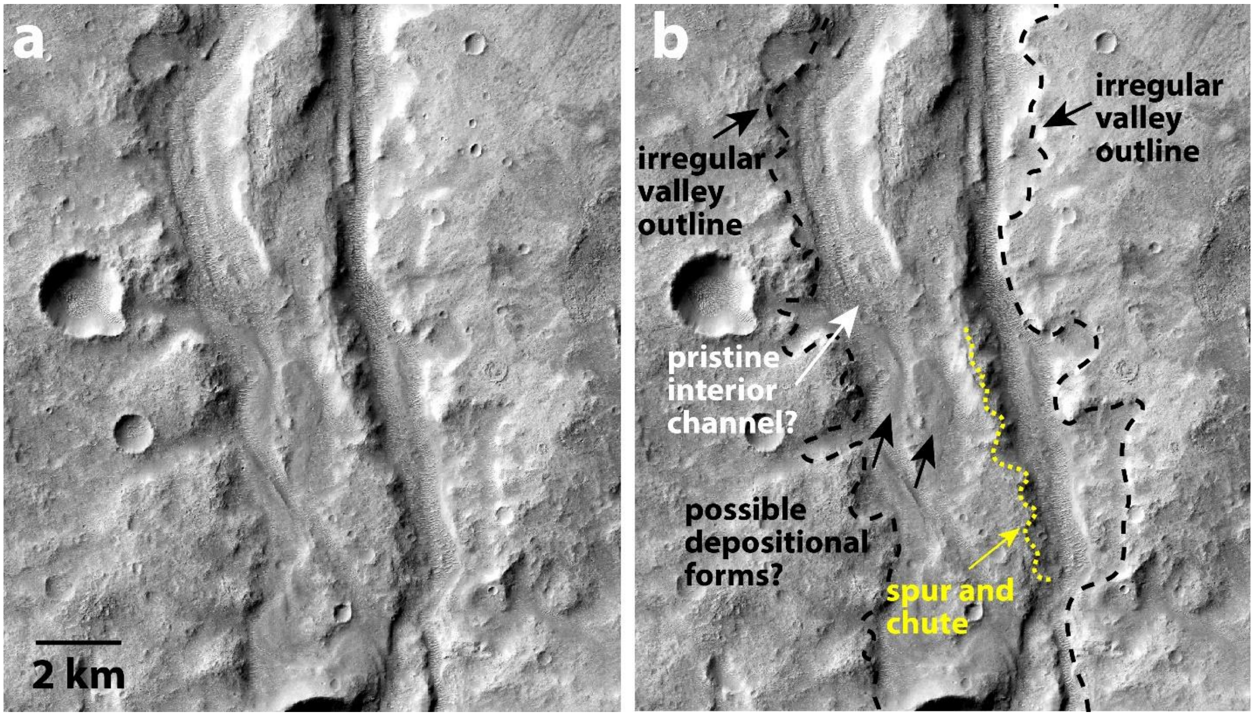

Figure 7. **a**) Unannotated and **b**) annotated view of Samara Valles ~150km south of Jones (see Figure 2 for context). The valley margins (black dashed lines) along this portion of Samara are irregular and spur and chute (yellow dotted line) morphology is present that is reminiscent of degraded valleys. Rounded lighter-toned lobes (black arrows) on the valley floor may be evidence of pristine depositional forms, and the valley floor to the north (downstream direction) may be more pristine (white arrow). Subframe of the MurrayLab_CTX_V01_E-020_N-24_Mosaic data (Dickson et al., 2018) centered near 22.3S, 340.2E. North is towards the top.

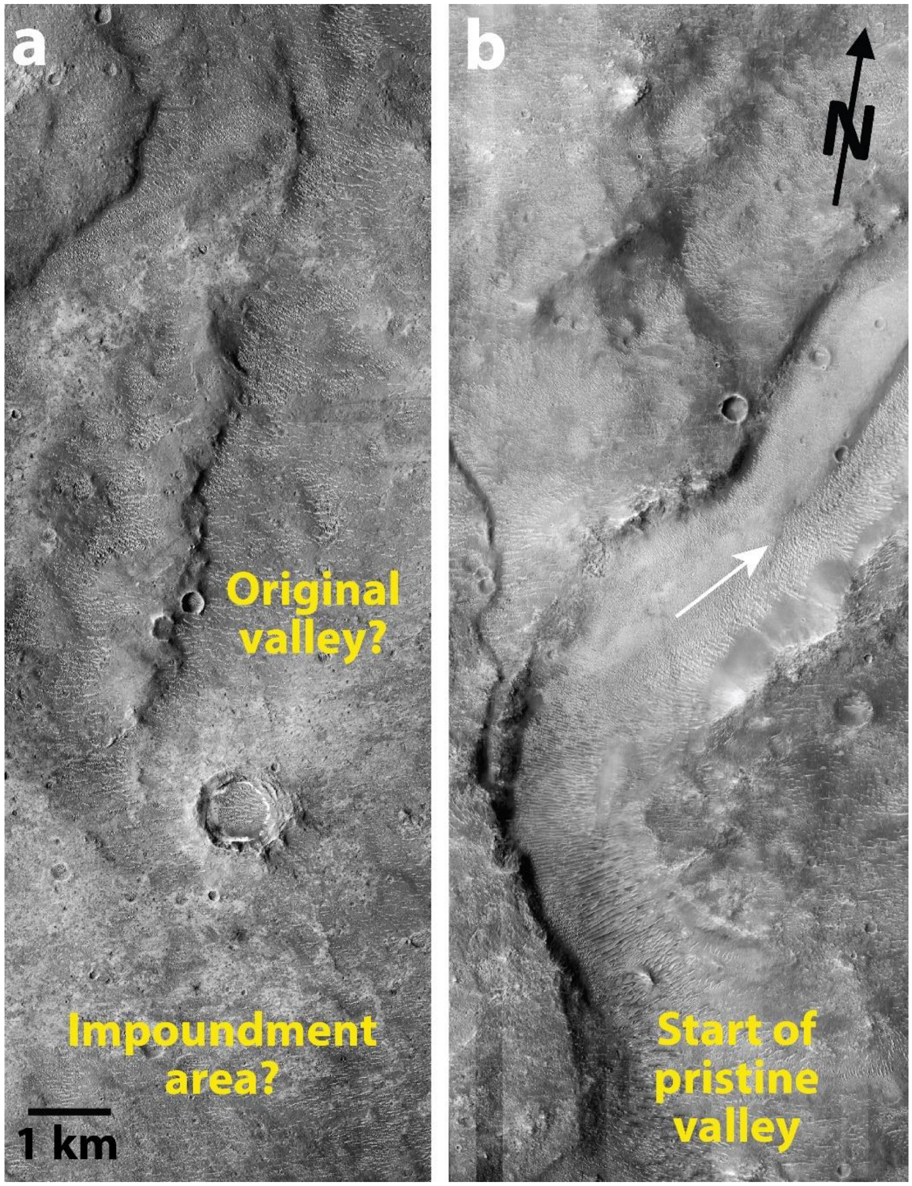

Figure 8. The relatively pristine valley is much larger where it emerges from the northeastern end of the upper basin, and it maintains a large cross-section downstream and beyond the lower basin (see Figures 2 and 4 for context). It is possible that the origination of the relatively pristine valley from the upper basin follows some or all of the original course of Samara Valles that facilitated the course of water through and downstream of the upper basin divide. White arrows indicate downstream direction. HiRISE images **a**) ESP_064749_1600_RED and **b**) ESP_074140_1605_RED with image resolutions of 0.50 m-pixel scale.

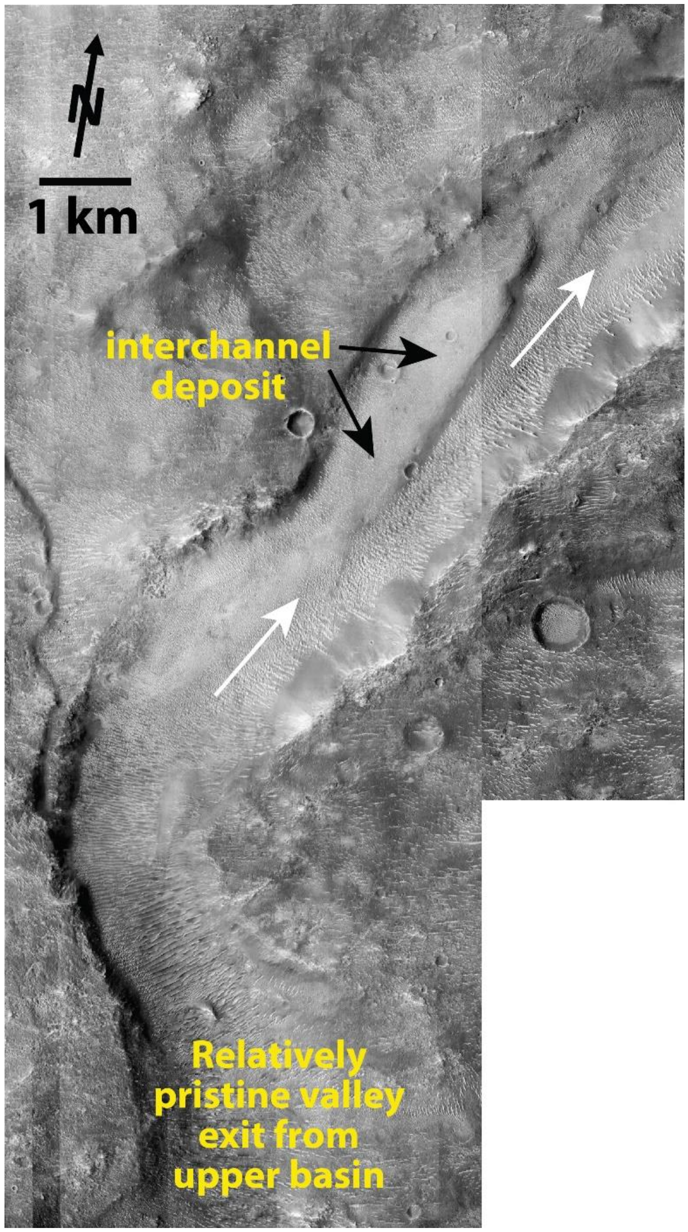

Figure 9. Downstream or northeast of the upper basin and immediately west of the crater, Samara Valles is well-incised and preserves interior deposits (black arrows) associated with earlier discharge or depositional bars related to discharge along the valley to the north (white arrows denote downstream flow direction, see Figures 2 and 4 for context). HiRISE images ESP_075142_1605_RED (0.25 m-pixel scale) and ESP_074140_1605_RED (0.50 m-pixel scale). Center of image is 19.5°S, 338.7°E.

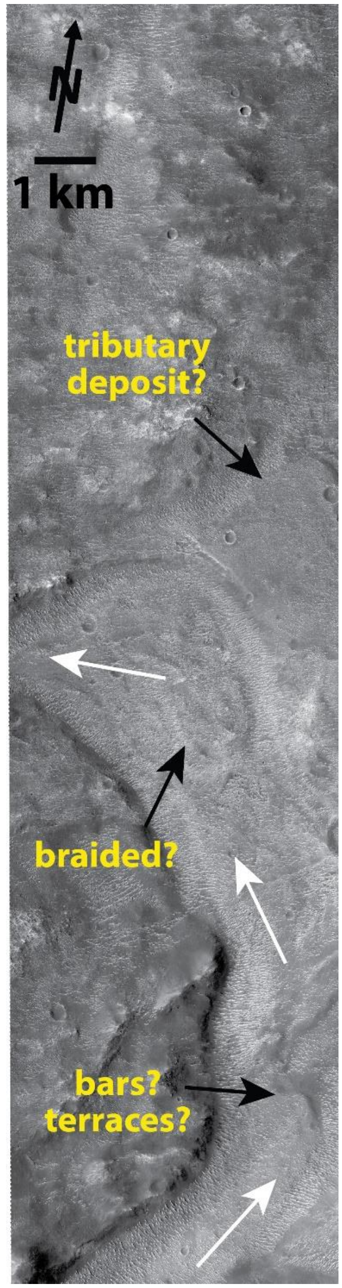

Figure 10. As the relatively pristine valley makes its closest approach to Jones and turns to the west, there are a series of forms along the floor that resemble a braided pattern and a bench or terrace marking entry of a possible tributary along a topographic low off the western flank of Jones (see Figures 2 and 4 for context). White arrows denote downstream flow direction. HiRISE image ESP_074997_1605_RED (0.50 m-pixel scale). Center of image is 19.2°S, 338.8°E.

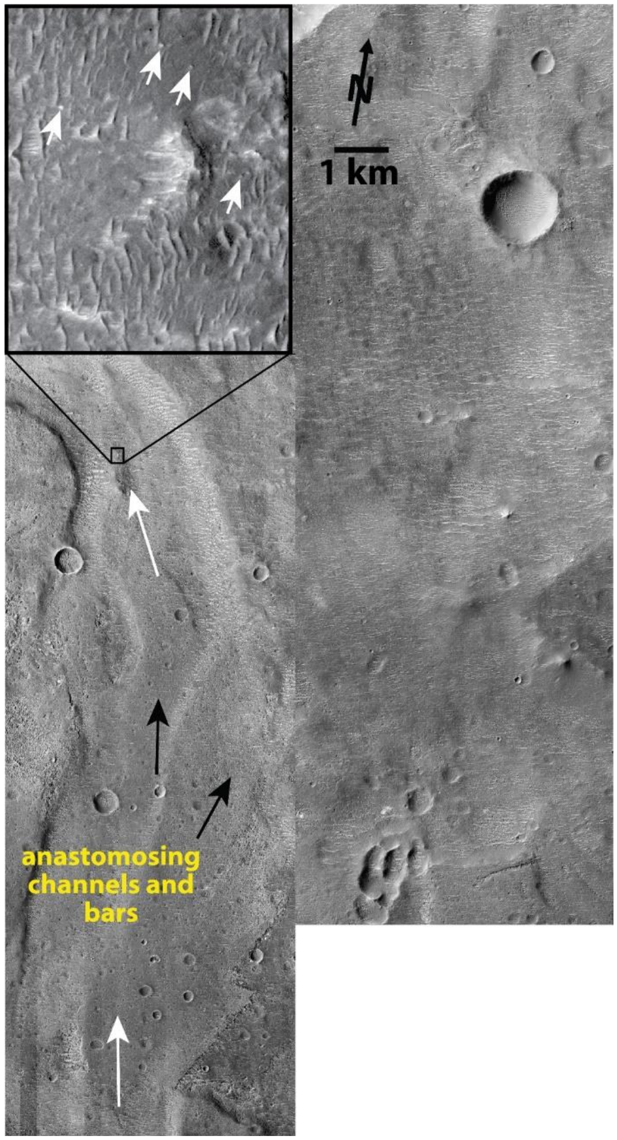

Figure 11. The expression of the valley changes again further north where it enters the lower basin (see Figures 2 and 4 for context) and becomes shallower and wider with multiple interior channels and overlapping fan-like depositional features. White arrows indicate downstream direction of flow. HiRISE images (McEwen et al., 2007) ESP_074285_1610_RED (left) and PSP_001982_1610_RED (right). Resolution of both images is 0.50 m-pixel scale. Inset shows large blocks (e.g., arrows) near the downstream end of the lower basin fan that supports high rates of discharge during the drainage of the basin (HiRISE ESP_074285_1610_RED, inset image is ~180 m across).

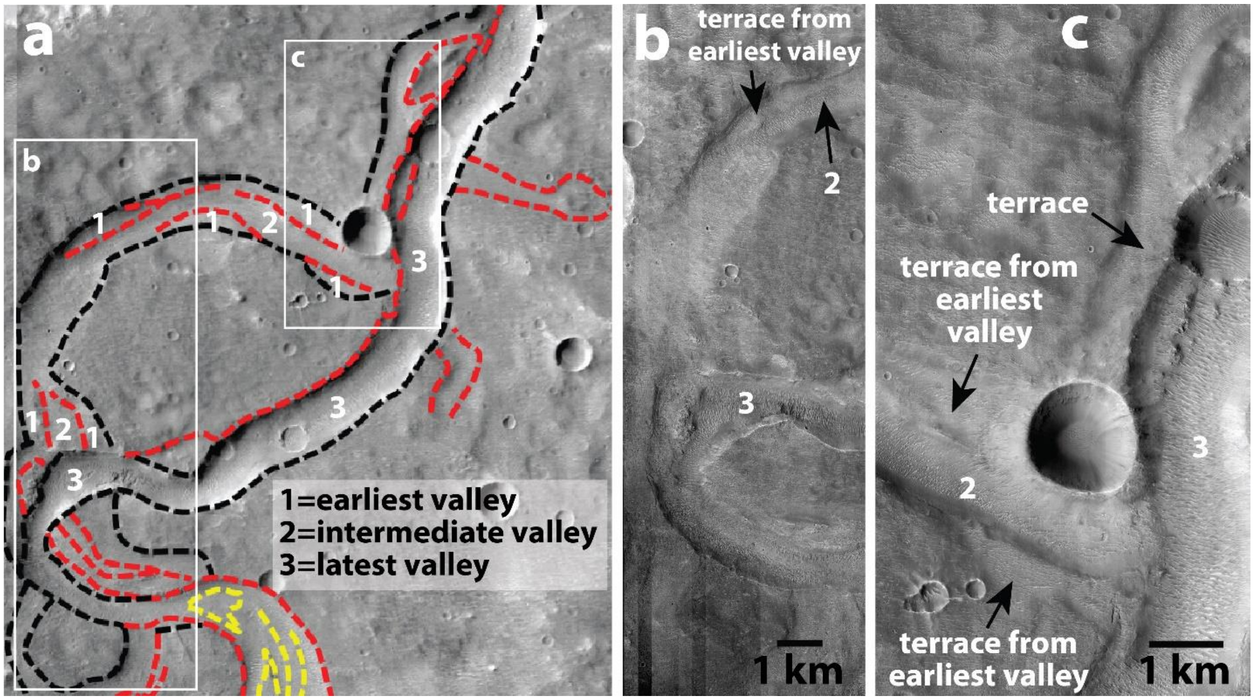

Figure 12. a) Early discharge from the lower basin flowed north, but segments were abandoned as the valley more deeply incised (earliest/oldest valley ("1"), intermediate valley ("2"), latest/youngest valley ("3"). Multiple terraces (red dashed lines) are also visible (see Figures 2 and 4 for context). Flow into multiple exits from the lower basin became consolidated into a single channel that more deeply down cut and left terraces and the higher segments abandoned. Boxes indicate location of (b) and (c). CTX image P02_001982_1611_XI_18S021W is ~17 km across (5.16 m-pixel scale). HiRISE images (McEwen et al., 2007) **b)** ESP_073995_1610_RED (0.50 m-pixel scale) and **c**) ESP_074496_1610_RED (0.25 m-pixel scale). North is toward the top.

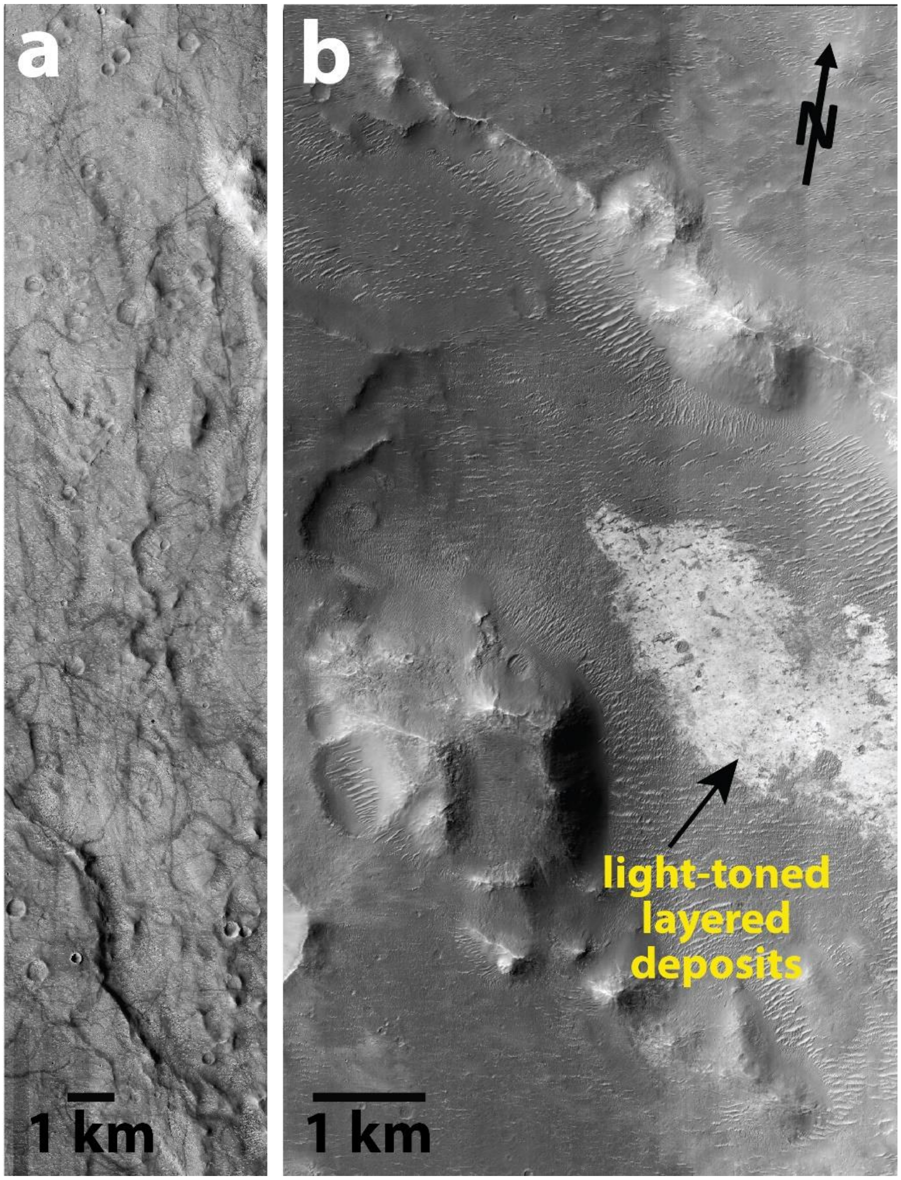

Figure 13. a) Further north, the expression of the valley becomes broader in CTX images, but the valley appears shallowly incised, rough, and irregular in HiRISE images (see Figure 2 for context). HiRISE image (McEwen et al., 2007) ESP_073863_1620_RED (0.50 m-pixel scale). **b**) Local occurrences of layered, relatively brighter deposits occur locally, typically in alcoves to the side of the main channel (see Figure 2 for context). HiRISE image ESP_046011_1620_RED (0.25 m-pixel scale).

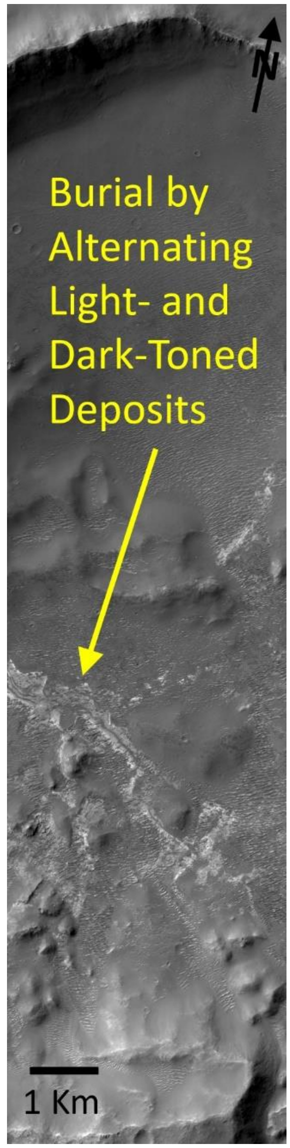

Figure 14. Valley expression much further to the north is muted and possibly related to alternating relatively dark and light-toned deposits that appear flat-lying and can be traced for kilometers around the margin of a crater that has been breached by late discharge from the valley (see Figure 19 for context). Such alternating relatively light and dark toned layered deposits are common on Mars, but here they appear associated with drainage into the crater via the wall breach by the valley on the eastern side. The valley takes on a more degraded appearance just downstream of the partially filled crater. Portion of HiRISE image ESP_027431_1650_RED (with a 0.50 m-pixel scale resolution).

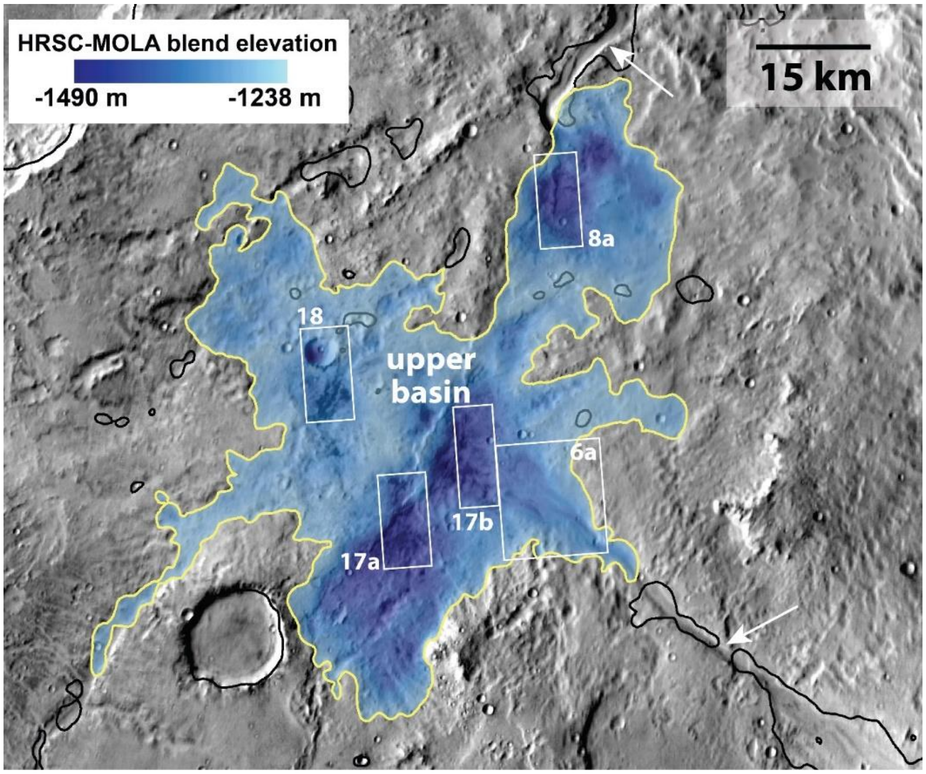

Figure 15. Location and approximate extent of upper basin along Samara Valles (white arrows) (see Figures 2 and 3 for context). Approximate surface of impoundment for the basins (outlined in yellow) is based on the -1275m MOLA contour (black lines). An estimated 46 km^3 of water likely filled the upper basin (approximate center is 20.1°S, 338.6°E) that lies upstream of most of the relatively more pristine valley segments that incise Jones crater ejecta and continue further downstream. Such a large volume of water may have accumulated via downslope migration of water/melting ice on and perhaps more importantly within and beneath the Jones crater ejecta where it then accumulated in the basin along the axis of the Chryse trough (see Figure 3 for context). This water may have been subsequently released downstream via overtopping and incision of the confining divide at the northeast end of the basin, thereby accounting for rapid incision of the relatively pristine valley segments. Box indicates location of Figures 6a, 8a, 17a, 17b, and 18. Base is THEMIS daytime IR with basin depth elevations from HRSC-MOLA blended topography. North and downstream towards the top.

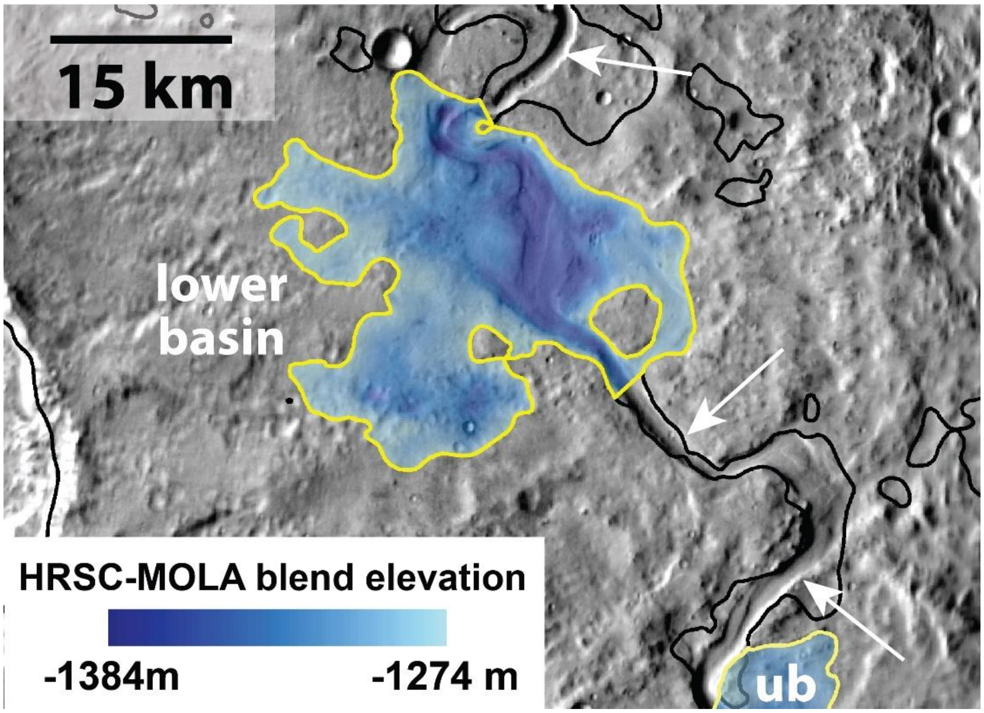

Figure 16. Location and approximate extent of lower basin along Samara Valles (white arrows) (see Figures 2 and 3 for context). Approximate surface of impoundment for the basins (outlined in yellow) is based on the -1275m MOLA contour (black lines). An estimated 7 km^3 of impounded water likely filled the lower basin (approximate center is 18.9°S, 338.4°E, see Figures 2 and 3 for context) that lies downstream of most of the well-incised, more relatively pristine valley segments incising Jones crater ejecta. In contrast to the upper basin (ub, Fig. 15), the valley expression is more continuous across this smaller basin which terminates into a series of anastomosing segments where exiting and draining further north (e.g., Figure 11). Water draining into the basin from the south probably overwhelmed the smaller basin and resulting in only temporary storage before overtopping created the anastomosing segments downstream. Base is THEMIS daytime IR with basin depth elevations from HRSC-MOLA blended topography. North and downstream towards the top.

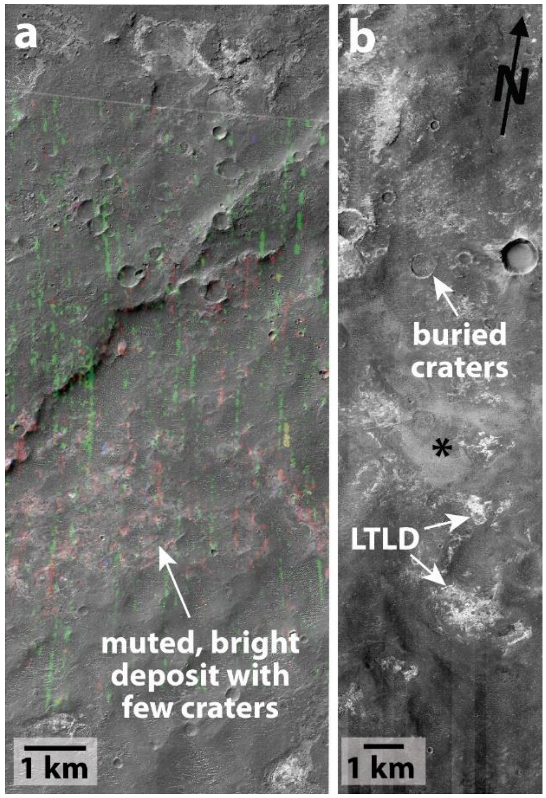

Figure 17. **a)** Floor of upper basin is not incised and there is no expression of the relatively pristine entry valley or associated the lobate deposits (see Figures 2 and 4 for context). The basin floor displays muted-to-bright-layered deposits that are Mg-Fe phyllosilicate-bearing in CRISM data (red and green areas to the right of the ridge on left image, CRISM image FRT00017BA7_07_IF164L_TRR3 overlain on HiRISE image ESP_017304_1595 (0.25m-pixel resolution) bounded by angled white lines near top and bottom, see text for discussion). **b)** Partially buried craters (e.g., top of image on right) and other morphologies, such as a generally muted texture, and outcrops of finely bedded, relatively brighter deposits (light toned layered deposits, LTLD, indicate deposition occurred on the ejecta lining the basin (**Fig. 4**). Area of central impoundment indicated by "*". HiRISE image (McEwen et al., 2007) ESP_075986_1595_RED (0.50 m-pixel scale).

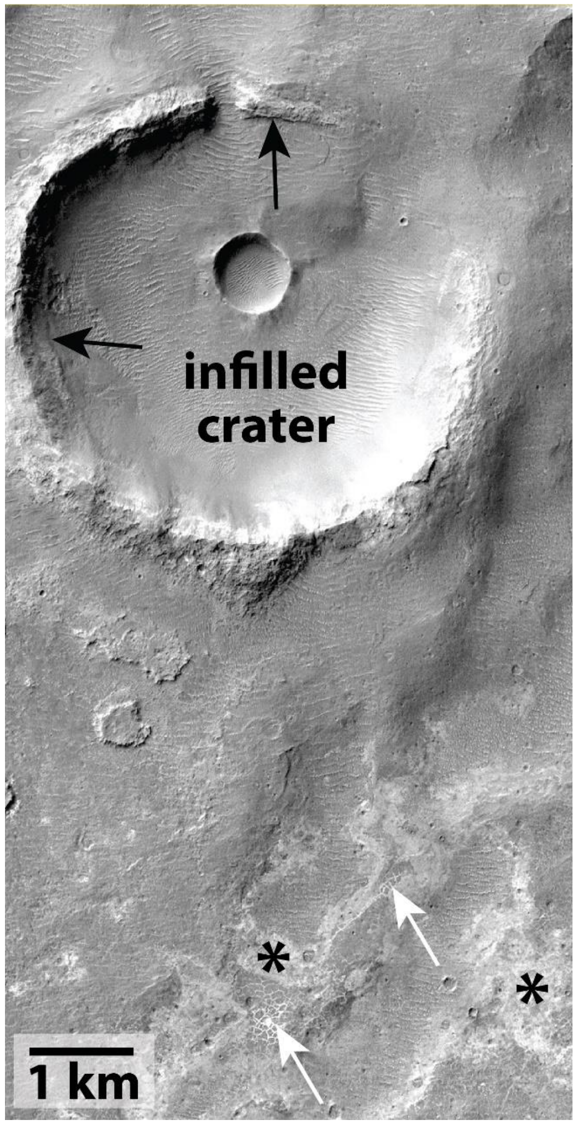

Figure 18. The floor of the upper basin displays relatively light-toned layered deposits ("*") and polygonal fractures (white arrows) (see Figures 2, 4, and 16 for context context). In addition, craters on the basin floor near the divide are partially filled (e.g., larger crater on right side) and have erosional benches (black arrows) cut into their walls that is consistent with erosion along a shoreline. Subframe of CTX image (Malin et al., 2007; Dickson et al., 2018) F18_042767_1592 with (~6 m pixel-scale resolution). North is towards the top.

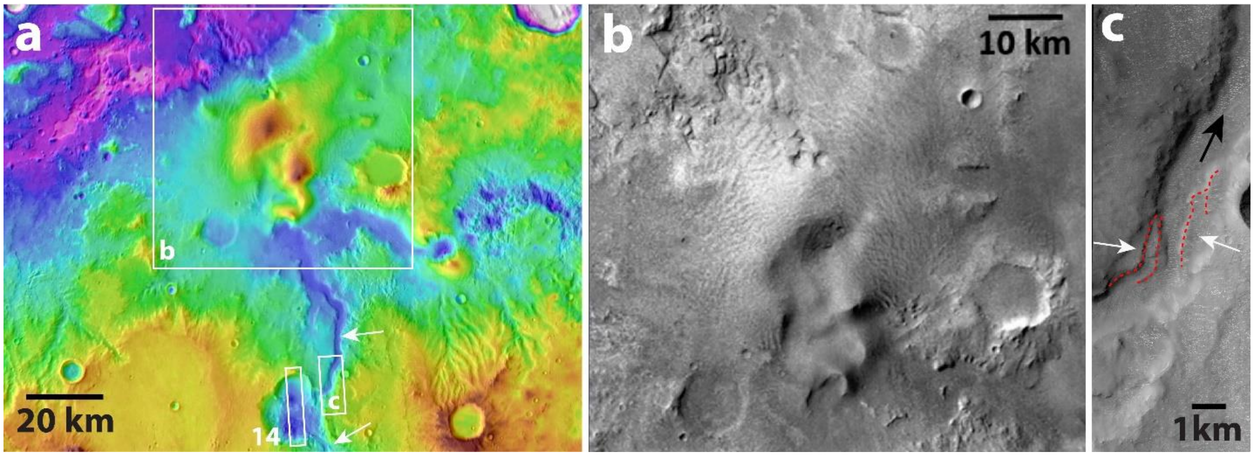

Figure 19. **a**) An Amazonian volcanic center formed along distal Samara Valles (white arrows) just prior to where the valley entered into Margaritifer basin (see Figure 2 for context). It is possible that associated volcanic deposits (ash) were redistributed to the south and partially buried the distal valley segment. Boxes indicate location of (b) and (c) and Figure 14. MOLA (Smith et al., 2001) over THEMIS Day IR data (Smith et al., 2001; Christensen et al., 2001; Edwards et al., 2011). **b**) Volcanic center along northern end of Samara Valles. THEMIS Day IR data (Christensen et al., 2001; Edwards et al., 2011). **c**) Valley appearance as seen in HiRISE (McEwen et al., 2007) is more degraded north of the crater in Figure 14 and looks more like the degraded segments to the south of the Jones crater ejecta deposit (Fig. 5). Although probable terraces (dashed red lines) are observed along the sides of the valley in the vicinity (flow direction indicated by red arrows), interior surfaces appear muted and buried. ESP_077173_1650_RED (0.5 m-pixel scale resolution). North is toward the top in all images.

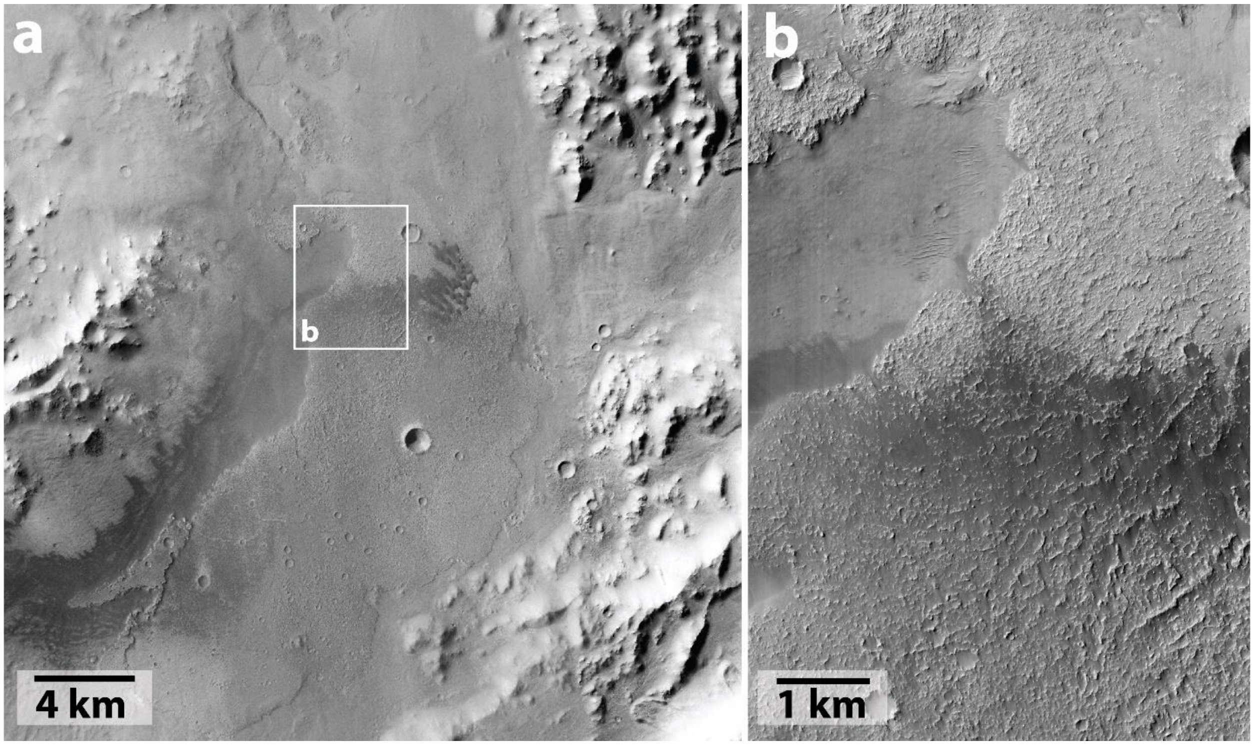

Figure 20. **a**) A lobate deposit on the southeast floor of Jones crater (see Figure 2 for context) bears similarities to lobate deposits associated with fluidized flow around the exterior of Hale crater that were emplaced there following impact melting of ice during and just after impact. Unlike the Hale deposits, however, the only possible example at Jones is within the crater, lacks well-defined arcuate transverse ridges, and expresses only limited digitate terminus around the margin. There is not an obvious exposed volcanic source vent for the Jones deposit, but it could be buried by younger alluvium (middle) or it could be a deposit of impact melt. Subframe of CTX mosaic with ~6 m pixel-scale resolution (Malin et al., 2007; Dickson et al., 2018). Box indicates location of panel (b). **b**) HiRISE image ESP_019440_1610_RED (McEwen et al., 2007) with a (0.25 m pixel-scale resolution). North is towards the top.